Norwegian University of
Science and Technology

Initial Studies of Strontium Titanate Substrates and Room Temperature Deposited Titanium Dioxide Thin Films

Erling Hannaas

Master of Science
Submission date: July 2017
Supervisor: Turid Worren Reenaas, IFY

Norwegian University of Science and Technology
Department of Physics

Abstract

To create doped titanium dioxide (TiO_2) thin films for use in intermediate band solar cells, it is important to be able to deposit thin films of high quality. To achieve this, substrates with surfaces of high quality is needed. Often, preparation is needed to get the correct termination on the substrate surface. HF etching is a widely used method for preparation of strontium titanate substrates, but it is both expensive and challenging, so we have tried using a different approach.

STO substrates have been prepared for deposition of TiO_2 thin films using three different methods. One used acetone and isopropanol to wipe the substrates, another used heat annealing at 1000 °C for an hour before being washed in an ultrasonic deionized water bath for 30 seconds. The third method used the same steps as the second, but repeated them twice (referred to as waterleaching), resulting in well-defined atomic planes. Substrates prepared by waterleaching have been studied before the treatment, straight after the treatment and one, two, three and six weeks after the treatment using atomic force microscopy (AFM). Untreated, newly treated and nine weeks old treated STO substrates were studied using electron microscopy (SEM), energy dispersive X-ray spectroscopy (EDS) and X-ray photoelectron spectroscopy (XPS).

AFM gave STO substrate surface roughness measurements ranging from (61 ± 3) pm to 123.5 pm, with a tendency of increasing roughness as time passed. Line scans over the atomic planes showed that the height of each plane was approximately in integer or half integer values of the STO lattice constant, meaning that the substrates were not completely TiO_2 terminated even after waterleaching. Still, XPS measurements showed that waterleaching did in fact increase the TiO_2 termination at the substrate surface to a limited extent.

TiO_2 thin films were deposited on untreated, newly treated and nine weeks old treated STO substrates by both pulsed laser deposition (PLD) and electron beam physical vapour deposition (EBPVD) at room temperature, due to a malfunctioning substrate heater in the PLD. The deposition rates of the PLD deposited thin films were calculated from profilometer measurements of the thin film thickness and were found to range from 4.58 pm/pulse to 6.04 pm/pulse. EDS scans of all six thin films showed that the oxygen content in the PLD deposited thin films was a lot higher than in the EBPVD deposited thin films.

As expected, X-ray diffraction showed the TiO_2 thin films to have no, or low, crystallinity. XPS measurements of TiO_2 thin films deposited on by PLD and EBPVD on newly treated STO substrates and by PLD on a silicon substrate, showed that the thin film composition was more dependent on the deposition method used than on what type of substrate was used. This was further confirmed by EDS-measurements.

Front: $2\,\mu m^2$ atomic force microscopy image of a strontium titanate substrate.

Sammendrag

For å lage dopede titandioksidtynnfilmer (TiO_2-tynnfilmer) til bruk i mellombånd-solceller (IBSC), er det viktig å kunne produsere tynnfilmer av høy kvalitet. For å oppnå dette trenger man substrater med god overflatekvalitet. Ofte trengs det da å gjennomføres preparering, for å oppnå den ønskede overflatetermineringen. HF-etsing er en mye brukt metode for preparering av strontiumtitanatsubstrater (($SrTiO_3$/STO)-substrater), men det er både dyrt og utfordrende, så vi har forsøkt å bruke andre metoder.

STO-substrater har blitt preparert for deponering av TiO_2-tynnfilmer ved hjelp av tre ulike metoder. I en ble aceton og isopropanol brukt til å tørke av substratene, i en annen ble substratene plassert i en ovn på 1000 °C i en time før de ble renset i et ultrasonisk deionisert vannbad i 30 sekunder. Den tredje metoden brukte de samme stegene som den andre, men de ble gjentatt to ganger (dette blir referert til som vann-etsing), som resulterte i veldefinerte atomplan. Substratene som ble preparert ved hjelp av vann-etsing har blitt studert før behandlingen, straks etter behandlingen, en, to tre og seks uker etter behandlingen ved hjelp av atomærkraftmikroskopi (AFM). Ubehandlede, nybehandlede og ni uker gamle behandlede STO-substrater ble studert ved hjelp av elektronmikroskopi (SEM), energidispersiv røntgenspektroskopi (EDS) og røntgenfotoelektronspektroskopi (XPS).

Ved hjelp av AFM målte vi STO-substratoverflatens ruhet til å variere mellom 61 ± 3pm og 123.5pm, med en tendens som tilsa at ruheten økte etterhvert som tiden gikk. Linjeskanning over atomplanene viste at høyden til hvert plan var tilnærmet en hel- eller halvtallig verdi av STO-gitterkonstanten, hvilket betydde at substratene ikke var fullstendig TiO_2-terminert, selv etter vann-etsing. Likevel viste XPS-målinger at vann-etsingen faktisk hadde økt graden av TiO_2-terminering på overflaten, til en viss grad.

TiO_2-tynnfilmer ble deponert på ubehandlede, nybehandlede og ni uker gamle behandlede STO-substrater ved hjelp av både pulsert laserdeponering (PLD) og fysisk elektronstråledampdeponering (EBPVD) ved romtemperatur, på grunn av en substratovn som ikke fungerte i PLD-oppsettet. Deponeringsraten til de PLD-deponerte tynnfilmene ble beregnet fra profilometermålinger av tynnfilmtykkelsene og ble funnet å variere fra 4.58 pm/pulse til 6.04 pm/pulse. EDS-skanninger av alle seks tynnfilmene viste at oksygeninnholdet i de PLD-deponerte tynnfilmene var betydelig høyere enn i de som var deponert med EBPVD.

Som forventet viste røntgendiffraksjonsmålinger av TiO_2-tynnfilmene at de hadde ingen, eller lav, krystallinitet. XPS-målinger av TiO_2-tynnfilmene deponert ved hjelp av PLD og EBPVD på nybehandlede STO-substrater og PLD på et silisiumsubstrat, viste at andelen av ulike materialer tynnfilmene besto av, var mer avhengig av deponeringsmetoden enn av hvilken type substrat tynnfilmene var deponert på. Dette ble ytterligere bekreftet av EDS-målinger.

Preface

This master thesis contains the work of a student during the spring of 2017 at the Norwegian University of Science and Technology on substrates for use in pulsed laser deposition experiments and deposition of titanium dioxide thin films. During the process, I have learned several techniques for advanced, and less advanced, characterization of samples, mostly at NTNU NanoLab, and I would like to thank all of the engineers that have helped me in my training there.

Ingeborg-Helene Svenum at SINTEF and Sverre Vegard Pettersen at NTNU were of great help with XPS training and discussions. I would also like to thank PhD candidate Thomas Brakstad for his collaboration and great scientific discussions, as well as laboratory help, and for always being willing to help me out, even when he had much more important things to do. Next, I would like to thank my supervisor, Associate Professor Turid Worren Reenaas, for doing her best in guiding me onwards whenever there were setbacks and challenges, for scientific discussions, help with writer's block and guidance throughout the entire process. Finally, I would like to thank my family, for their prevailing support through many years at the university, and for sponsoring motivational food and beverages in the final weeks before the master thesis deadline.

Erling Hannaas
Trondheim, July 6, 2017

Contents

Abstract . . . iii

Sammendrag . . . v

Preface . . . vii

1 Introduction **1**

2 Introduction to Deposition of Titanium Dioxide on Strontium Titanate **3**

2.1 Crystal Structures and Lattice Matching . . . 3

2.2 Substrate Preparation . . . 4

2.2.1 Literature Study of Strontium Titanate Preparation . . . 4

3 Experimental Techniques **7**

3.1 Thin Film Deposition . . . 7

3.1.1 Electron Beam Physical Vapour Deposition . . . 7

3.1.2 Pulsed Laser Deposition . . . 8

3.2 Characterization . . . 10

3.2.1 Atomic Force Microscopy . . . 10

3.2.1.1 Tapping Mode . . . 11

3.2.1.2 Contact Mode . . . 11

3.2.1.3 Non-Contact Mode . . . 12

3.2.2 Scanning Electron Microscopy . . . 12

3.2.3 X-ray Photoelectron Spectroscopy . . . 13

3.2.4 Energy Dispersive X-ray Spectroscopy . . . 13

3.2.5 Profilometry . . . 14

3.2.6 X-ray Diffraction . . . 14

4 Experimental Details **15**

4.1 Substrate Preparation . . . 15

4.1.1 Strontium Titanate . . . 15

4.2 Thin Film Deposition . . . 16

4.2.1 Electron Beam Physical Vapour Deposition . . . 16

4.2.2 Pulsed Laser Deposition . . . 16

4.3 Characterisation . . . 18

4.3.1 Atomic Force Microscopy . . . 18

4.3.1.1 Image Processing . . . 18
4.3.2 X-ray Photoelectron Spectroscopy . . . 19
4.3.3 Scanning Electron Microscopy and Energy Dispersive X-ray Spectroscopy 21
4.3.4 Profilometer . . . 21
4.3.5 X-ray Diffraction Settings . . . 21

5 Results **23**
5.1 Substrate Studies . . . 23
5.1.1 Surface Topography and Roughness . . . 24
5.1.1.1 Untreated Substrates . . . 24
5.1.1.2 Acetone and Isopropanol Treated Substrates . . . 24
5.1.1.3 Weak Waterleached Substrates . . . 26
5.1.1.4 Waterleached Substrates . . . 26
5.1.2 Surface Composition of Untreated Substrates . . . 32
5.1.3 Bulk and Surface Composition . . . 34
5.2 Thin Film Studies . . . 38
5.2.1 Deposition Rate of PLD Deposited TiO_2 Thin Films . . . 38
5.2.2 Surface Composition . . . 38
5.2.3 Crystallinity . . . 40
5.2.4 Surface Structure and Thin Film Composition . . . 40

6 Discussion **55**
6.1 Substrate Surface Studies . . . 55
6.1.1 Roughness and Inclination . . . 55
6.1.2 Surface Composition . . . 57
6.1.3 Bulk and Surface Composition . . . 58
6.1.4 Improvements . . . 59
6.2 Thin Films . . . 59
6.2.1 Thickness and Deposition Rate . . . 59
6.2.2 Surface Composition . . . 60
6.2.3 Crystallinity . . . 60
6.2.4 Surface Imaging and Bulk and Surface Composition . . . 61

7 Conclusion **63**

8 Suggestions for Future Work **65**

Bibliography **66**

A SEM Images of Surface Particles at TiO_2 Thin Films **71**

Chapter 1

Introduction

Solar cells are becoming increasingly important as a source of clean, renewable energy on a world-wide basis [1]. While the technology has existed for several decades, there is a great potential for improvements in regards to solar cell efficiency, building materials, life time, production cost and methods, and so on. Third generation solar cells, taking advantage of the properties of intermediate band semiconducting materials, are currently being researched all over the world [2], including here, at the Norwegian University of Science and Technology. This work is but a small cog in the machine in the work for the years to come, and describes the initial research stages of substrates for use in pulsed laser deposition (PLD) experiments in addition to TiO_2 thin films grown at room temperature using two different methods. The field is new to our team, and routines need to be developed for efficient and reproducible production of thin films.

To create an intermediate band solar cell, one needs to synthesize a semiconducting material with an energy band within the bandgap [3]. The theoretical efficiency of such solar cells is calculated to be 63.2 % and realizing this potential would make for great strides in the field of renewable energy [4] One way of creating the intermediate bands is to dope a material with some impurity. An advantage of such materials is that they might allow for sub-bandgap photons to be absorbed, greatly increasing the electron flux from the valence band to the conduction band without reducing the output voltage, according to Fara et. al. [5].

The overall goal of our PLD experiments is to create an oxide based IBSC of great efficiency, by growing highly crystalline thin films, with different dopants in different concentrations. Initially, we hope to achieve this by using PLD to create a doped TiO_2 thin film, as research has pointed towards co-doped TiO_2 having potential for intermediate bands [6], giving an IBSC with a theoretical efficiency of up to 52.7 % [7].

To grow anatase thin films by PLD, most research teams use temperatures ranging from 500 °C to 800 °C. This is done using a substrate heater at the back of the sample stage. Sadly, after some time with studies of substrate preparation and working with laser alignment, we found that the heater in our PLD system was broken and could not be fixed for several months. The focus of my work was then shifted towards the substrates, with the goal of char-

acterizing different preparation methods that could be used for later experiments. Three different methods were tested, and the one that proved most promising was characterized for three weeks using atomic force microscopy, mainly to research if and how the substrate surface decayed over time. If they did not decay, we would have the opportunity of preparing a lot of substrates at the same time, saving us a lot of work in the future, as substrate preparation can be quite time consuming.

Scanning electron images were taken of STO substrates before, straight after and many weeks after the preparation. These substrates also had their composition checked using energy dispersive X-ray spectroscopy (EDS). To get a better understanding of the surface composition on the substrates, we recruited the help of SINTEF, and performed X-ray photoelectron spectroscopy.

After imaging substrates that had been prepared using different methods with AFM, and doing studies of the substrates prepared by the method we found worked the best for a few weeks, the AFM broke down, and again, the focus of my work had to be shifted. This time to the deposition of thin films using PLD and electron beam physical vapour deposition (EBPVD) and research the difference of these thin films, deposited on the substrates we had prepared earlier. As the PLD heater did not function and the EBPVD do not allow for high temperatures, all the thin films were deposited at room temperature, and we tried to use pressures that were as close as possible in the different instrument main chambers. Due to the low temperature, the deposited thin films were expected to have a low crystalline quality, but the experiments helped us develop methods for deposition either way. The deposited TiO_2 thin films were characterized using gracing incidence X-ray diffraction (GI-XRD), and as expected, the thin films were not crystalline. The thin films were then imaged using SEM and the thin film composition was researched using EDS. Finally, we used XPS to research the surface composition of the TiO_2 thin films deposited on newly prepared STO substrates by PLD and EBPVD, in addition to a thin film deposited on a silicon substrate.

Chapter 2

Introduction to Deposition of Titanium Dioxide on Strontium Titanate

The chapter opens with an explanation of why it is important to know the lattice constants of both the substrate material and the deposition material when one is doing pulsed laser deposition (PLD) experiments. As this work is centred around TiO_2, the lattice of TiO_2 is discussed in further detail later in the same section, in addition to the structure of strontium titanate ($SrTiO_3$, STO). To get an overview of what other research teams have done, a literature study of STO substrate preparation is also presented.

2.1 Crystal Structures and Lattice Matching

All crystalline materials have their atoms organized in some orderly fashion on a microscopic scale, and different materials may have their atoms and molecules arranged in different types of lattices [8]. Exactly what type of lattice a material has, is dependent on a lot of factors. The crystal lattice may determine properties such as conductivity, reflectiveness, piezo-electrical properties and much, much more. What we are interested in for the purposes of our team, is to find a material that is very well suited for creating oxide based, doped, intermediate band solar cells.

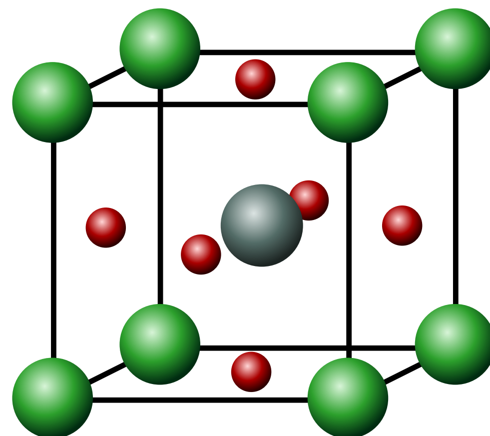

Figure 2.1: Example of a perovskite, in this case $SrTiO_3$, where the green atoms represent strontium, the red, oxygen, and the grey titanium.

STO, also known as tausonite, is a perovskite (see figure 2.1), with lattice constant, a, ranging from $a = 3.905$ Å to $a = 3.913$ Å [9, 10]. If the STO substrate is cut in a (100) orientation, the surface lattice should match quite well

with that of anatase TiO_2, assuming that the STO substrate have been prepared in the correct way [9]. TiO_2 can have both rutile, anatase and brookite structures, with rutile being the most common form found in nature [9]. The first two of these structures are tetragonal, while the latter is orthorhombic. The difference between the anatase and the rutile structures is that they have different values for their lattice constants. Anatase has $a = 3.7845\,\text{Å}$ and $c = 9.5143\,\text{Å}$, while rutile has $a = 4.5937\,\text{Å}$ and $c = 2.9587\,\text{Å}$ [9]. The lattice constant values, a, for STO and anatase TiO_2 are quite similar, meaning that it should be possible to create thin films by deposition of one material onto the other with a very tight fit between the materials [11].

2.2 Substrate Preparation

Before depositing a thin film on a substrate is important to have knowledge on the substrate surface, as this may influence the thin film one wants to deposit, in turn affecting the thin film properties [12, 13]. STO substrates are TiO_2 terminated only for a limited time after being prepared for deposition, depending on the preparation process [14]. A variety of instruments can be used to test whether the chosen preparation method has created a surface that only contains the wanted termination for the thin film deposition or not.

It is important that the roughness of a substrate does not exceed the roughness of a deposited thin film [13, 15]. In the starting phase of a deposition, the substrate surface may be affected in such a way that the roughness increases, so for a better deposition it is recommended that the surface roughness is lower than the expected thin film roughness.

2.2.1 Literature Study of Strontium Titanate Preparation

A method that has been widely used for substrate preparation is HF etching, where hydrofluoric acid (HF) is used to etch off atomic layers on the surface of a STO crystal to make it atomically flat, meaning that height differences are multiples of the unit cell height of the crystal in question [16–18]. A typical way of performing HF etching is to etch a substrate in a buffered HF-solution for some time. One may choose to anneal the substrate at a high temperature (see table 2.1 for some reference values) and giving it an ultrasonic bath in deionized water (DI water) to clean it off. Some do the annealing in vacuum with specific elements as a background gas [16–19], while others do it under atmospheric pressure [14, 20]. The heating time can vary greatly between different research groups, and everything from 1 h to 10 h have been used.

During the heat annealing process of the substrate, the mobility of the atoms in the upper layers of the sample is increased, and they start to move across the substrate surface. Parts of the sample where there have been trenches or valleys will now be filled by the atoms moving across the sample surface, and as this happens, the surface is flattened. As the sample cools down, the atoms will rest in their new positions and often this makes the substrate atomically

flat. The longer the substrates are annealed, the more time the atoms have to rearrange themselves, making for a flatter substrate when it cools down.

HF solutions can be rather expensive, and can be very dangerous in regard to HSE, so having some other way of preparing substrates would be advantageous. The team of Connell et. al. reports that a heat annealing and water leaching method may be used to create TiO_2 terminated STO substrates, without the use of HF [14].

Looking at figure 2.1, one can see that the STO crystal consists of layers of respectively strontium oxide (SrO) and titanium dioxide (TiO_2). Removing the strontium oxide layer will make the surface consist of a TiO_2 layer, well suited for deposition of TiO_2. A way of removing SrO is to take advantage of the fact that it is water-soluble; in other words, removing the SrO can be done by washing it off in water. This can be done by placing the substrate in an ultrasonic DI water bath for somewhere around 30 seconds [14].

As apparent from table 2.1 there is no standard for the preparation of STO, but the most common methods are mentioned in the table, except for the first one, of Connell et. al., being quite rare. There are those who have used entirely different methods, such as Laser Molecular Beam Epitaxy (MBE), where STO is used as a target that is deposited on a STO substrate before the deposition of a thin film [21]. Others, have cleaned of their substrates using soap water, ethanol, methanol and DI water [22].

Table 2.1: Examples of different preparation methods used on STO substrates. NS=not specified, Atm=atmospheric pressure. The ones who used water for cleaning off the substrates dried them off using N_2, if anything was specified.

Ref	HF	Anneal	Temperature [°C]	Time [minutes]	Pressure [mbar]	Gas	Water	Time [s]
[14]	No	Two times	1000	60	Atm	Air	Yes	30
[16]	Yes	Yes	927	120	$1.33 \cdot 10^{-5}$	O_2	No	•
[17]	Yes[1]	No	•	•	•	•	Yes	NS
[18]	Yes[2]	No	•	•	•	•	Yes	NS
[15]	No	Yes	950	120	10^{-10}	NS	No	•
[20]	No	Yes	1000	600	Atm	O_2	No	•
[22]	No	No	•	•	•	•	No	•
[23]	No	No	•	•	•	•	No	•
"	No	Yes	750-850	60	$1.33 \cdot 10^{-8}$	NS	No	•
"	No	Yes	800-1100	900	NS	O_2	No	•

[1] Done by using NH_4F with pH4.5 for 10 minutes
[2] "

Chapter 3

Experimental Techniques

This section describes details behind instruments used for deposition of thin films and some instruments that can be used to characterize them.

3.1 Thin Film Deposition

There are several ways of depositing thin films, with a wide variety of advantages and disadvantages. The following sections presents the two methods used in our experiments.

3.1.1 Electron Beam Physical Vapour Deposition

The following section is based on [24]. One way of creating thin films is to use physical vapour deposition (PVD), in which one of the most used techniques is electron beam PVD (EBPVD). It functions by bombarding a target material, such as metals or oxides, with a beam of high energy electrons, excited from a tungsten filament in a high vacuum chamber (see figure 3.1). The electron beam is directed by the use of a magnetic field in such a way that it hits the wanted position on the target. As this happens, the target is heated in the area surrounding the beam, and atoms are evaporated into the chamber. This effect is partly due to the low pressure in the chamber, as well as the high temperature in the target, freeing the atoms. The electrons give almost all of their energy to the atoms, giving them the energy to escape the target and evaporate into the camber. The atoms that are spread from the target may be deposited on a substrate by placing this at an appropriate distance from the target.

EBPVD processes takes place in a vacuum chamber, normally at low pressures (below $4.0 \cdot 10^{-4}$ mbar) [24]. If the chamber pressure becomes too high, it will hinder the electron beam and stop the entire process. Temperatures in the chamber may vary, but as the pressure is very low, it is more meaningful to consider the substrate temperature. This may be regulated by placing a heater near the back of the substrate holder.

A disadvantage of EBPVD is the great limitations in the chamber pressure, which means that there are limited options for introducing background gas, or gasses, in the chamber during a deposition, limiting the possibilities for thin film composition variation as these

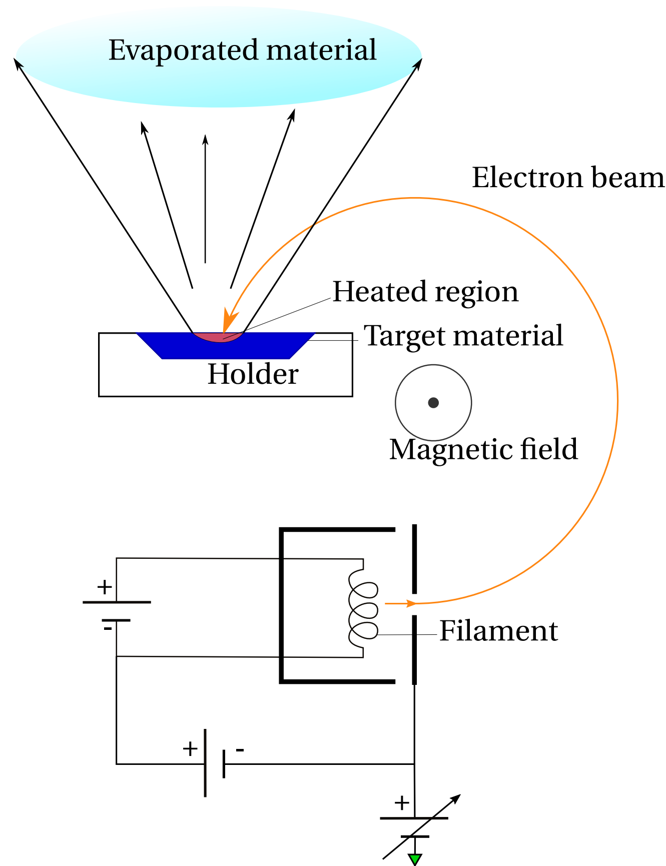

Figure 3.1: Principle of EBPVD. Electrons are excited from the filament and accelerated into a magnetic field, pointing up from the paper, bending the beam onto a target material placed in a holder. This heats up the target material, which is then evaporated into a vacuum chamber. Placing a substrate somewhere in the chamber allows the user to deposit monolayers and thin films of the target material on their chosen substrate.

background gases may greatly affect the deposited thin film. Another downside is that you have very little control over the behaviour of the evaporated material. It spreads through most of the vacuum chamber, which is why the filament and other instrument parts must be covered in some way. The large spread of the evaporated material means that the entire chamber will be covered in a thin film of the target material. This, in turn, may affect later depositions, so one should try to clean out the chamber at a relatively high frequency.

3.1.2 Pulsed Laser Deposition

The following section is based on [25]. In PLD one uses a high intensity collimated light source, or laser, to shoot short pulses (on micro or nanosecond scale) of light, with a specific wavelength, at a target material that is placed in a vacuum chamber. When the light pulses hit the target, material starts to evaporate, creating a plume of plasma. As the plume spreads, it can hit a substrate placed at a short distance (centimetre range) from the target, where the material may be deposited. An example of a PLD system is shown in figure 3.2. The deposited thin film may obtain a uniform crystal structure, depending on what target and substrate

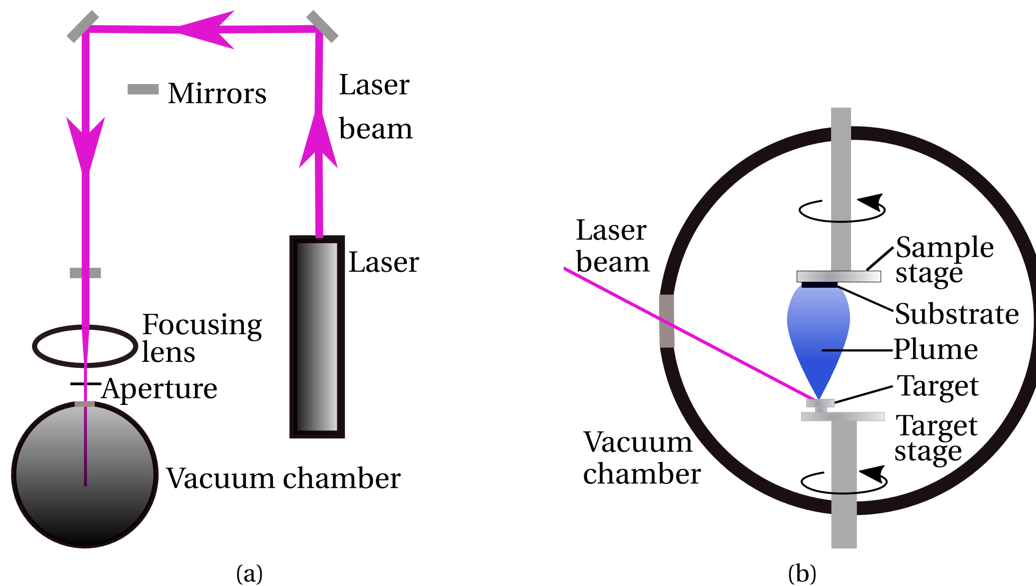

Figure 3.2: (a) shows the basic setup of a PLD system, where a laser shoots out collimated light via mirrors, through a focusing lens and an aperture, and passing a quartz glass as the beam enters a vacuum chamber. (b) is a description of such a chamber. The laser beam enters the chamber and hits a target, placed at the target stage (which may be rotated during the deposition). A plasma plume rises from the target and is deposited on a substrate placed at the sample stage (which may also be rotated).

material is being used, repetition rate, chamber pressure, temperature, laser wavelength and fluence (intensity per square centimetre). Pressure can be regulated by the introduction of a gas in the chamber, e.g. oxygen or nitrogen. This gas pressure affects the size and energy of the plume, regulating how much of the ablated material sticks to the substrate and in turn, the thickness of the thin film. The thickness of the thin film after a deposition correlates with the number of pulses that was shot at the target, and this is described by the deposition rate defined as the increase in thickness per pulse. Larger chamber pressure will make the plume smaller and less energetic and may stop the ablated material from reaching the substrate. However, if the particles in the plume have too much energy, they may knock off parts of the deposited thin film or not stick to the substrate at all, which also lowers the deposition rate.

PLD gives the user a relatively simple way of depositing thin films. All that is needed is a laser and a vacuum chamber. This simple set up means that PLD is one of the more reasonably priced ways of depositing thin films. Another great advantage of PLD is its possibilities when it comes to depositing thin films from different materials. It is fairly easy to change both the target and the substrate, giving the option of depositing a wide array of thin films in a relatively quick manner. The speed at which a thin film is deposited can be high, although this depends heavily on the target material, in addition to all the other factors mentioned above. A disadvantage of PLD is that what's happening inside of the plume is complex, but we don't always need to know. The energy of the plume can be regulated, using background pressure in the chamber, but it is difficult to control the plume in any other way. Another problem can be that the deposited thin film will not have the same thickness everywhere,

due to the shape of the plume (assuming that the substrate is flat). Because the properties of thin films vary with the thin film thickness, the PLD deposited thin film may have different properties at different locations on the same deposited thin film. In addition to this, thin films deposited by PLD have a limited size, due to the limitations of the plume size, which, in part, is caused by limitations in laser beam spot size.

3.2 Characterization

There is a wide variety of tools for characterization of thin films. Different microscope technologies include atomic force microscopy (AFM), optical microscopy and scanning electron microscopy (SEM). Elemental mapping of thin films and substrates can be done by X-ray photoelectron spectroscopy (XPS) and energy dispersive X-ray spectroscopy (EDS, EDX). Any possible crystal structure in the deposited thin film can be characterized using X-ray diffraction (XRD). Measurements of height profiles can be obtained using profilometry. Principles behind the characterization tools we have used is described in further detail in the following sections.

3.2.1 Atomic Force Microscopy

When characterizing a sample, the surface can be imaged using AFM. There are three modes under which AFM can be performed; contact mode, tapping mode and non-contact mode. The principle can be seen in figure 3.3, and can be described as follows: A tip attached to a cantilever is moved across a sample surface. As the topography of the sample changes, so does the Z-position of the cantilever. A laser beam is reflected off the back of the cantilever, and registered at a photodetector. The movement of the cantilever and the way the laser signal is registered, is dependent on the mode in which the instrument is working. When the tip has moved across a set length of the sample, you have scanned one line of the surface. Now, the cantilever/tip is moved a tiny distance in the XY-plane, and then it starts a new scan. After repeating this several times, the line scans can be put together to an image of the sample surface. As the tip is moved in three dimensions, the image can be viewed in the software as a three-dimensional image. In short, AFM uses contact forces, and not beams of light or particles such as electrons or ions, when creating an image. By scanning multiple lines very close together, the instrument can create a 3D mapping of the surface topography. The technology makes it possible to view sample surfaces all the way down to atomic level [26].

Depending on the properties of the sample you want to image, it is important to choose the correct tip and cantilever (see figure 3.4). If you have a harder sample, you would be best served with a harder tip and stiffer cantilever. This may be regulated by varying the width of the legs of the cantilever. Wider legs will make for a stiffer cantilever, and smaller for a softer one. In addition to this, it is important to consider the topography of your sample. If there

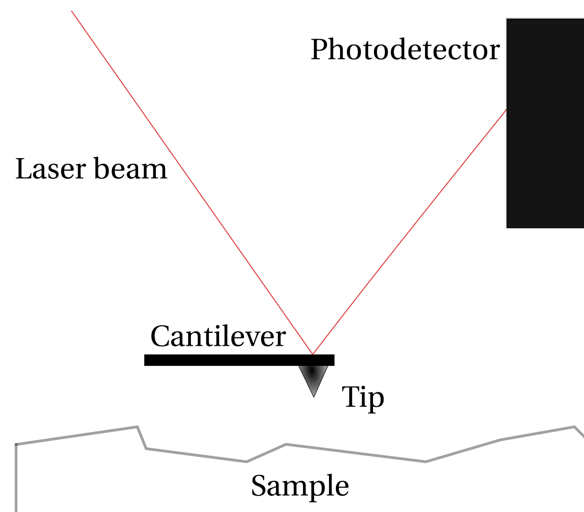

Figure 3.3: Principle of AFM. A laser is reflected off the back of a cantilever to which a tip is attached. The tip is moved across the sample surface, and a photodetector registers the changes in the laser signal.

are large variations on the sample surface, you will need to choose a cantilever that can move accordingly.

3.2.1.1 Tapping Mode

In tapping mode, the AFM tip is oscillated vertically as it is moved across the sample surface [26]. Forces between the sample and the tip, such as Van der Waals forces, electrostatic forces, etc. creates changes in the amplitude of the cantilever oscillation [28]. As these changes are registered in the photodetector, they are corrected to a setpoint value by moving the cantilever in the vertical direction by a piezo. The correction voltage is recorded, and a correlation factor in the software determines the height at the given location on the sample. A problem with this method is that the piezo is subject to nonlinearities due to hystereses, creep, drift, and aging effects [28].

3.2.1.2 Contact Mode

Contact mode AFM works by dragging the tip across the sample, being in contact the whole time [29]. The laser reflecting off the back of the cantilever hits the photodetector, and as the tip moves up and down over the surface of the sample, the light beam moves on the photo detector. This signal is a representation of the height at the point where the tip is located and is a direct way of mapping the cantilever deflection. The final image is the product of all needed such line scans. Due to the fact that there is physical contact between the tip and the surface, this method may damage the samples, and the tip is damaged more easily than in the other modes.

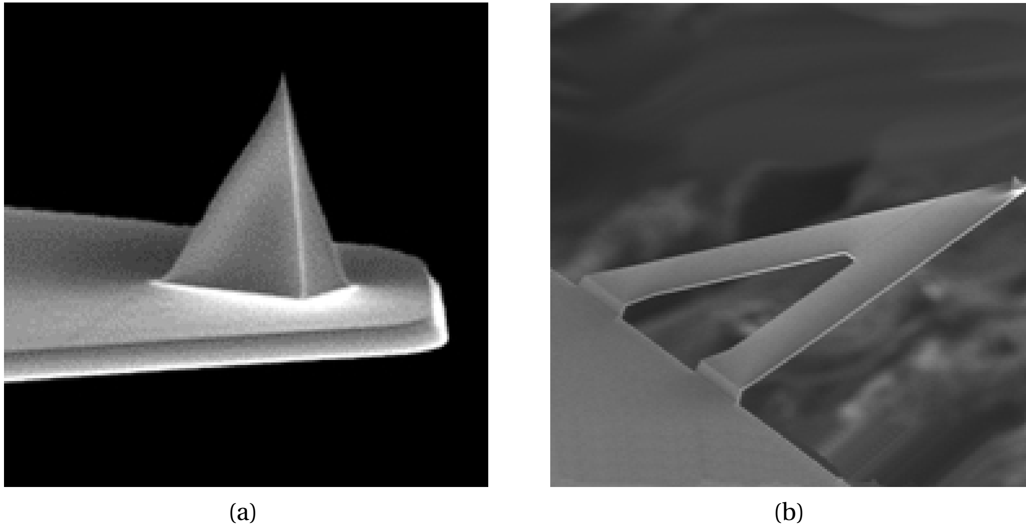

(a) (b)

Figure 3.4: Image of tip (a) and cantilever (b) produced by Bruker for use with their Scan-asyst mode AFM [27]. Both parts are made from silicon nitride. The cantilever has a thickness ranging from 0.6 µm to 0.7 µm. The tip has a maximal radius of 12 nm [27].

3.2.1.3 Non-Contact Mode

In this mode, the tip is moved to an order of Ångstrøms close to the sample surface, but never in direct contact. Next, the cantilever is set to oscillate at a certain amplitude and frequency. Forces that can affect the tip at these distances, such as the van der Waals force, affect the amplitude and/or the frequency of the oscillation. The image is created from these force interactions. An advantage of this mode is that the tip has a very long lifetime, however, the method does not allow for large features on the sample surface.

3.2.2 Scanning Electron Microscopy

Optical microscopes are not suited for looking at samples on a micro- or nano-scale, due to their limitations in wavelengths. SEM, however, makes it possible to look at samples in these ranges, and create detailed images of the sample topography as well as giving a nice image of material structure. The SEM consist of an electron cannon that shoots a beam through lenses before hitting the sample one wants to examine, producing new electrons with energies corresponding to the sample material. Detectors surrounding the sample register the energies of the particles escaping the sample that was hit [30].

There are several technologies that can be used for SEM imaging, one of which is using back scattered electrons (BSE). These electrons are produced when the electrons hit the sample and scatter back from some point near or at the surface. Using BSE, one obtains a good elemental contrast, meaning that different elements are easy to tell apart. Heavier elements appear brighter due to the fact that they better scatter the incoming electrons. The downside to BSE is that the resolution obtained is lesser than in e.g. secondary electron imaging (SE) [31]. When imaging with BSE's, some SE's may interfere and cause the image to get smeared.

Some of the electrons from the incident beam will penetrate deeper into the sample than other. Another factor greatly influencing the resolution of the BSE images is the angle of the incident beam [30].

3.2.3 X-ray Photoelectron Spectroscopy

Based on the works of Einstein in 1905, XPS have made for great advances in the characterization of materials. It is a method that is excellent at defining surface composition in samples, and is one of the most used methods for such characterization. The technique characterizes the composition of the surface approximately 10 nm into the sample, assuming that at least 0.05 % of a material is present [32].

The basic principle is as follows. A photon, a massless particle, transfers all its energy to an electron that is bound to an atom in the sample we want to study. If the energy of the photon is sufficient, that is, greater than the electron binding energy, the electron is ejected from the atom [8]. The remaining kinetic energy of the electron is characteristic for the atom to which it was bound, and it is this kinetic energy that is possible to measure. The different kinetic energies the electrons have when being ejected are listed in tables, making it easy to match the measurements with specific elements. The energy of the scattered electron can be calculated from

$$K_e = E_\gamma - E_b - \Phi,$$

where K_e is the kinetic energy of the scattered electron, E_γ is the energy of the incoming photon, E_b is the binding energy of the electron and Φ is the work done by the instrument.

A limitation in the instrument can be the size of the X-ray beam hitting the sample. Where a larger beam might excite more electrons, the measurements may have a lesser definition, whereas a smaller beam might give good measurements, but might not cover enough of the sample to characterize all elements present.

The three most common ways of presenting XPS data is with an energy distribution of all electron emissions within a specified energy range, spatial distribution of the electrons emitted, showing the elemental distribution and, finally, depth distribution [32].

3.2.4 Energy Dispersive X-ray Spectroscopy

To examine the material composition of a sample, one might use energy dispersive X-ray spectroscopy (EDS, EDX). This technique is made possible from the fact that different elements have different peaks in the electromagnetic emission spectrum. The principle of operation is as follows: A beam of high energy particles, such as electrons or protons, are shot at a sample. This, in turn, excites the electrons in the material. As the electrons fall down to lower energy states, the excess energy is released in the form of X-rays. The energy of the X-rays is characteristic for the material from where they originated, and can be measured by a spectrometer, making it possible to map the elements present in a sample. The strength

of the output signal is not only dependent on the incident beam, but also the materials in the sample. Some materials have a higher absorption than others, meaning that the output signal is not necessarily representative of the true elemental distribution in the sample.

3.2.5 Profilometry

To determine the profile of a sample surface an instrument, aptly named a profilometer can be quite useful. This instrument drags a very small stylus across a sample, registering shifts in height as if moves along. The technology can be used to make a profile of larger samples than AFM in a relatively short time, but the technology only allows for one line scan at a time, and do not have the option of a complete surface mapping [33].

3.2.6 X-ray Diffraction

To characterize the lattice of a crystal, XRD is a very useful tool [34]. The technique was developed for solids in the mid-1900s and is based on the understanding of electron interactions in solids developed in the early 1900s [35]. The principle is as follows. X-rays, having wavelengths in the Ångstrøm range, will be scattered by the electrons of the atoms in a material. As a beam of X-rays hits a sample, most of these scattered electromagnetic waves will cancel each other out through destructive interference, but some will have constructive interference (when the path difference of two parallel incoming beams is an integer number of wavelengths) in directions determined by Braggs law,

$$2d\sin\theta = n\lambda,$$

where d is the distance between the diffraction planes, θ is the incident angle, n is an integer and λ is the wavelength of the X-rays. By evaluating the angle θ, finding a value for d is quite simple. If you do measurements on a single crystal, few diffraction peaks will appear, and so, measuring might be difficult. This can be made easier by creating a powder from the single crystal. The powder will give many more diffractions in different directions, making for diffraction circles in 2D.

A problem with XRD on thin films is that the incoming X-rays may penetrate the thin film and the measured value for θ will be more representative for the underlying substrate than the deposited thin film. To measure on the deposited thin film alone, one might do gracing incidence XRD (GI-XRD), in which the incident angle is far smaller than in normal XRD, meaning that the incoming beam mainly diffracts with the thin film, making diffractions patterns characteristic for the thin film, and not the underlying substrate [36].

Chapter 4

Experimental Details

Preparation of STO substrates was performed using three different methods. One was prepared using acetone and isopropanol and the other two methods used a combination of heat annealing and an ultrasonic deionized water (DI water) bath.

To deposit thin films on the STO substrates, we used both pulsed laser deposition (PLD) and electron beam physical vapour deposition (EBPVD). We deposited TiO_2 thin films on three different substrates using both methods. The characterization of both the STO substrates and the TiO_2 thin films was conducted using a wide variety of instruments, including AFM, SEM, XPS, EDS and XRD.

4.1 Substrate Preparation

Different substrates may require different preparation methods, so in this section we will only expand upon our STO substrates. These were purchased from the MTI corporation, and they were created using single crystal STO produced in Japan.

4.1.1 Strontium Titanate

STO (100) substrates were prepared for deposition in three different ways with the purpose of making them atomically flat. We prepared one substrate by wiping it with acetone and isopropanol and bathing it in an ultrasonic bath in DI water for approximately 20 s.

The next substrates were prepared using heat annealing and an ultrasonic DI water bath. The STO substrates were placed on quartz glass in an oven filled with air at atmospheric pressure, and annealed at 1000 °C for an hour before we let it cool down inside the oven, that had been switched off after the hour was over. Next, we washed it off in an ultrasonic DI water bath (this method will later be referred to as *weak waterleach*). The final substrates were treated by the same annealing and leaching procedure, but the process was repeated twice (this method will later in the paper be referred to as *waterleaching*).

Initial studies of the substrates and the works of Connell et. al. [14] helped us decide to use the waterleached substrates in our future experiments. As our initial plan of creating co

deposited PLD thin films did not include detailed surface studies of the substrates, the first substrates we prepared were characterized by AFM immediately after the preparation, before resting in air for sex weeks and being characterized yet again. We prepared new substrates and performed AFM on them after one week, two weeks and three weeks. We were halted in our studies after the third week due to the AFM malfunctioning. Nine weeks after the first substrate preparation, we prepared new substrates by water leaching. These new substrates will later be referred to as new, while the ones we prepared first will be referred to as old. Untreated substrates will be referred to as untreated.

4.2 Thin Film Deposition

We wanted to create thin films using two different techniques under as similar conditions as possible, as this would isolate the difference in the thin films as a function of the deposition method used. By using both untreated, new and old substrates, we could compare them later and check if the preparation had affected the thin film deposition and/or surface in any way.

4.2.1 Electron Beam Physical Vapour Deposition

The E-beam PVD (EBPVD) used was manufactured by Pfeiffer, and is called Vacuum Classic 500. Setting the acceleration voltage to 8.00 kV and the beam current to 40 mA, and increasing the pressure in the main chamber to $p_{\mathrm{EBPVD}} = (1.1{\pm}0.1){\cdot}10^{-4}$ mbar (recommended by the instrument manufacturer [37]) by introducing oxygen as a background gas, all the while without any form of external heating mechanism, the TiO_2 deposition was started. The thickness of the thin film was measured by the instrument as the thin film was growing, and the deposition was stopped when the instrument registered a thickness of 300 nm. The crystal health of the thickness measurer was at 95 % during the entire deposition, during which, the deposition rate varied between 1.5 Å s^{-1} and 2.3 Å s^{-1}. After the deposition, the substrates still appeared as transparent.

4.2.2 Pulsed Laser Deposition

As the heater was not functioning, we deposited a total of four thin films at room temperature, three on the untreated new and old substrates, and one a silicon substrate. The latter was used to get an idea of the deposition rate compared to old experiments done using similar parameters on our PLD setup [38]. Before the deposition started, the pressure in the chamber was $p_{\mathrm{PLD},1} = (1.0{\pm}0.1){\cdot}10^{-4}$ mbar, but as soon as the deposition started this increased to $p_{\mathrm{PLD},2} = (1.1{\pm}0.1){\cdot}10^{-4}$ mbar. The pressure was obtained by letting the main chamber turbo pump rotate at its maximum velocity of 820 Hz and by introducing 1.5 sccm of oxygen into the chamber. The substrates were placed as shown in figure 4.1 and the sample stage was rotated at a constant velocity of $v_s = 40\,^{\circ}\mathrm{s}^{-1}$. This was done to ensure that

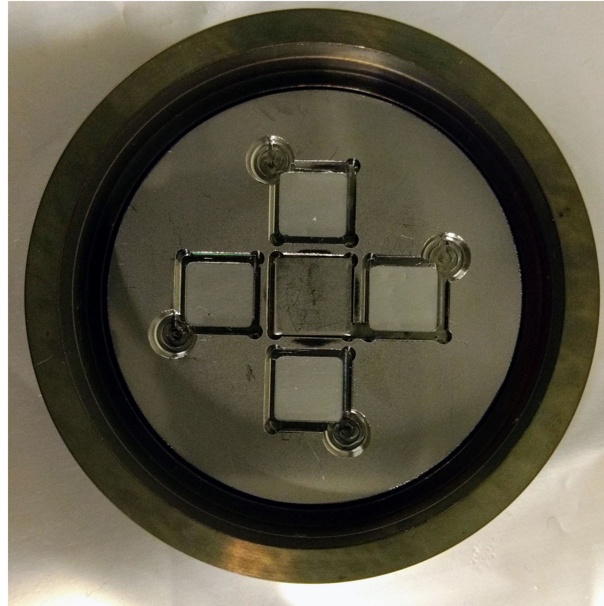

Figure 4.1: Si substrate(lower) and three STO substrates in the sample stage, after a PLD deposition. The middle position is filled by a steel placeholder, to avoid contamination of the substrate heater during the deposition.

the all substrates were subject to the same conditions during the deposition, as the plasma plume was centred at one substrate, and not in the middle of the sample stage, to obtain a higher deposition rate on the individual substrates and creating a gradient if we want to do this in later depositions.

Our PLD was a set up made by NeoCera, of the United States. We used a laser fluence of approximately $(1.0\pm0.1)\,\mathrm{J\,cm^{-2}}$ and a laser wavelength of $\lambda = 248\,\mathrm{nm}$. Before the deposition started, a pre-ablation of the TiO_2 target was done, by shooting 3000 10 Hz pulses at the target while it was rotated with a maximal target carousel velocity of $10\,^\circ\mathrm{s^{-1}}$ and a minimal target carousel velocity of $3\,^\circ\mathrm{s^{-1}}$, to ensure similar surface conditions on the whole target before the deposition started. The target carousel velocities make the target carousel move faster toward the middle and slower towards the edge of the target, to ablate the target more evenly than if the carousel was moving at a constant velocity. The same conditions for the carousel movement were used during the thin film deposition.

The deposition rate of TiO_2 on a gallium arsenide substrate standing still in our PLD set up, with a O_2 background pressure of 0.12 mbar at room temperature and a fluence of $3.56\,\mathrm{J\,cm^{-2}}$, has been calculated to be 36.7 pm/pulse when the substrate is placed at the top of the plume, and the plume hits in the centre of the substrate [38]. Seeing as our substrates were rotated and thus did not experience the same amount of deposition per pulse, we estimated that, to grow a 300 nm thick thin film, we would need approximately 24 000 pulses.

4.3 Characterisation

The substrate and thin film characterization was done using a wide array of instruments, most of which were provided by NTNU NanoLab. The following section describes the instruments in some detail as well as the characterization procedures we used them for.

4.3.1 Atomic Force Microscopy

Images of substrate surfaces were taken using AFM, and the Gwyddion software was utilized for image processing [39]. At first, we had other plans with these substrates than AFM studies, so initially they were only characterized to check if they appeared as flat and ready for deposition. Then they were stored in air for six weeks before being imaged yet again. New substrates were then prepared using water leaching, and studied for three weeks straight, before the AFM broke down. The image size was varied between 13 μm^2, 2 μm^2 and 500 nm^2, as these sizes were found to cover the most interesting features on the STO surface. The AFM used was manufactured by Veeco Metrology and it is called diMultimode V. The first few times we used AFM, we only imaged one area, but after some evaluation, we changed this, and started taking three images at different parts of the substrates every time we went to the lab. This was to make sure that an image was representative for most of the substrate, and that we what we were seeing was not an anomaly. The substrate itself was taped at its edges to a magnetic holder, as shown in figure 4.2. Line scans were performed to check the surface termination of the substrates. Planes of integer STO lattice constant value would indicare TiO_2 termination, whereas half integer step heights would indicate a mix of SrO and TiO_2 termination at the surface. The line scans were performed over few steps, to improve the step height measurement and make the plots easier to read.

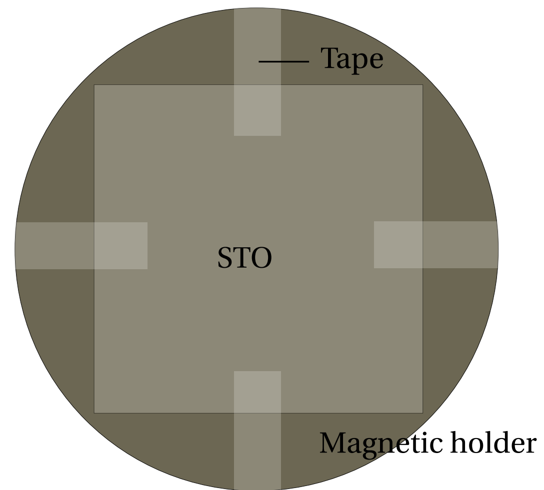

Figure 4.2: Illustration of how the STO substrate was attached to the magnetic plate holding the substrate still for AFM imaging. The tape, mounted between the magnet and the substrate was double sided and used at the edges to try and avoid contamination of the substrate as much as possible, in case of later use in other instruments.

4.3.1.1 Image Processing

The process of manipulating the AFM images to best present the relevant data is presented in figure 4.3 and is described as follows: The raw images (see figure 4.3a) were flattened in Gwyddion by using "median levelling of the rows in the image" (see figure 4.3b). Next, the

images were cleaned up, if needed, using the "correct horizontal scars (strokes)" function (see figure 4.3c). The result of all these operations, and changing the scale and colours, was an image with several overlapping planes (see figure 4.3d). The function "Level data by fitting a plane through three points" was used on a single of these planes, shifting the entire image into a series of flat planes lying on top of one another (see figure 4.3e). To easily compare images taken at different locations on the substrate surface, the same colour scale was chosen for the images we wanted to compare. Lastly, some images were treated with the function called "Basic Filters: mean, median, denoise, ..." to make the steps smoother and measurements of the step size easier (see figure 4.3f).

4.3.2 X-ray Photoelectron Spectroscopy

The elemental mapping of the untreated, new and old substrate surfaces was done using a XPS manufactured by Kratos Analytical called Axis Ultra DLD. Seeing as STO is an almost completely isolating material the substrates were mounted on glass plates to avoid charging effects (see figure 4.4). This was done by using carbon tape to attach a glass plate to the holder, upon which the substrates were attached using even more carbon tape, making sure that none of the tape was sticking outside of neither the glass plate nor the substrates. Next, the holder was introduced to the XPS main chamber, with a pressure of $6.67 \cdot 10^{-9}$ mbar, and we calibrated the focusing height of each substrate by scanning the carbon peaks and maximizing the area under the intensity curve.

The next step was to run a survey over the entire spectrum to see where we found peaks. To check for charge drifting effects, we did three survey scans on each substrate, and checked if the peaks were at the same position in all of them. The survey scan of the old substrate was performed with an anode electrical power of 100 W, whereas the surveys of new and untreated were performed with a power of 150 W to increase the signal strength. All the survey scans were performed with a pass energy of 160 eV, hybrid lens mode, an acquisition time of 121 s, in energy steps of 1 eV and with an activated charge neutraliser, with a filament current of 1.6 A, charge balance of 3.6 V and filament bias of 1.2 V. By comparing the scans from all three substrates, we saw that the peaks were located at the same binding energies, so we could move forward with these scan parameters for all the substrates. We did not see any drift effects on any of the substrates. We searched for titanium, oxygen and strontium on each substrate. We found a peak for oxygen in the range from 535 eV to 520 eV, titanium in the range from 464 eV to 448 eV and strontium in the range from 135 eV to 126 eV. Next, we wrote a program that scanned these three areas in steps of 0.1 eV ten times each. The acquisition time was 838 s, 510 s and 501 s for Sr, Ti and O respectively, and their dwell times was respectively 594 s, 298 s and 332 s. As the peaks were not found where we expected from tabular values, we also ran a scan over the adventitious carbon peak on all three substrates, to check how much the energy was shifted. The scan parameters for the carbon scans were as follows: Pass energy of 20 eV, hybrid lens mode, an acquisition time of 574 s and energy steps of 0.1 meV.

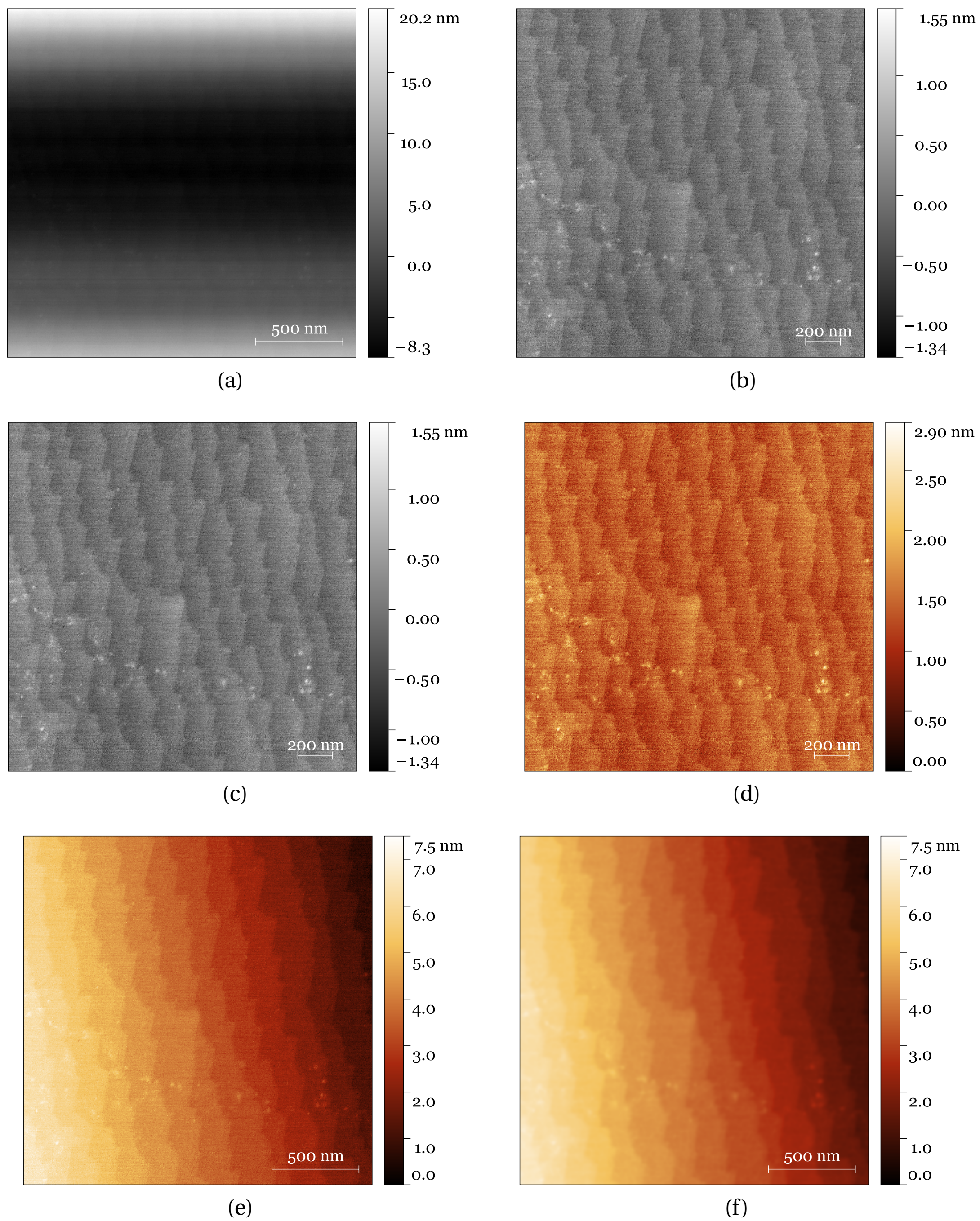

Figure 4.3: The process of image manipulation. (a) is the raw image, (b) is median levelled, (c) has scars and strokes removed, (d) adds colour and changes the scale bar, (e) levels data by fitting a plane through three points on the surface and (d) has been subject to "basic filters: mean, median, denoise, ...".

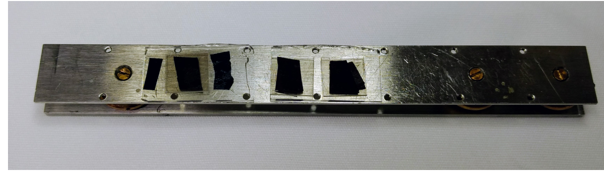

Figure 4.4: Three STO substrates mounted on a holder, ready for XPS. The substrates are attached with carbon tape (black) to glass plates, which in turn are attached to the sample holder with carbon tape.

4.3.3 Scanning Electron Microscopy and Energy Dispersive X-ray Spectroscopy

Both imaging and EDS of the substrates and thin films was done by using the SEM APREO with different acceleration voltages and currents to optimize the image quality of each individual substrate and thin film. Images were taken using secondary electrons. The SEM APREO was manufactured by FEI and has a theoretical resolution of 1 nm at 1 kV (material dependent) [40].

4.3.4 Profilometer

By using the Detak 150 profilometer to measure the thickness of the PLD deposited thin films, deposition rates of the TiO_2 thin films were calculated. The instrument uses a diamond tip stylus that it drags over the surface of the sample. The instrument was used to scan over edges at the PLD deposited thin films, as these had been partly covered during the deposition, making for a well defined edge. The EBPVD deposited thin films were not covered in any way during the deposition, and their thickness's could not be measured using the profilometer.

4.3.5 X-ray Diffraction Settings

GI-XRD was performed on all the deposited thin films with the same settings; an incident angle of 3° and angle 2θ from 20° to 61°. The resulting data was smoothed using a span of 3 in the Matlab function *smooth* and plotted in Matlab. Using `smooth(x,3)` takes the data point and the two data points surrounding it and averages them into a single value, making for a smoother plot, with reduced noise.

Chapter 5

Results

This section is divided into two parts. The first presents the results from the substrate studies; surface topography and roughness measurements by AFM on substrates prepared using different methods, and an AFM time study of a water leached substrate, as well as SEM images and EDS measurements of untreated, new and old substrates. The second part presents the results from our work with thin films. In this section, the focus lies not only on the surface, but also on the thin film composition and deposition factors. As in the first section, the surfaces have been imaged using SEM and composition have been studied by EDS. The surface composition of three of the thin films have been measured using XPS. Thickness measurements of the PLD deposited thin films were made using a profilometer, giving estimates for deposition rates on untreated, new and old STO substrates. Attempts were also made at characterizing potential crystal structures in the thin films using gracing incidence XRD.

5.1 Substrate Studies

This section presents AFM and SEM images of the substrates that had been prepared by different methods as well the surface of an unprepared substrate. EDX line scans gives an idea of the materials present in both an untreated, new and old waterleached substrate. XPS measurements gives a more detailed look at the surface composition of all of these three. Gwyddion was used to measure the roughness on all the substrates and the results are presented in table 5.1 and 5.2.

Table 5.1: Roughness of STO substrates prepared by different methods

Method	Time[weeks]	Roughness[pm]
Untreated	0	180±3
	6	61±3
Acetone and isopropanol	0	102±5
Weak waterleach	0	80±5

5.1.1 Surface Topography and Roughness

5.1.1.1 Untreated Substrates

Substrates that were only treated by an ultrasonic DI water bath for thirty seconds, which we call untreated, are presented in figure 5.1. Images 5.1a and 5.1b were taken not long after the DI bath, while 5.1c and 5.1d were taken after the substrate had been stored in air inside a small container for six weeks. Notice that the scale bar in figure 5.1b differs from the others. Setting the scale bar equal to the others rendered the image unintelligible. Figure 5.1a shows large defects of some material, formed as spires, protruding from the entire surface. In the lower left corner, there seems to be a couple of spires that have fallen over. Zooming in on one of the upright spires shows its general outline and some features (see figure 5.1b). It can seem as if there are points at the spire that are even lower than the surrounding, more uniform, surface. The same substrate, imaged six weeks later shows no sign of these spires. Figure 5.1d shows a general slanting nature to the substrate, where it appears as if layers of the material is lying on top of layers, with an increasing number of layers towards the left side of the image. The edges of the layers do not display high uniformity, as small parts of a layer can lie on top of a small part of the next layer, but most all lines are straight, and angles are, for the most part, 90°. The roughness was measured using Gwyddion with a result presented in table 5.1.

5.1.1.2 Acetone and Isopropanol Treated Substrates

The AFM image of the acetone and isopropanol treated substrate is shown in figure 5.2. The image appears to be flipped by 90° if we compare it to figure 5.1d. This is most likely due to the substrate not being in the same orientation as the other substrates when it was imaged in the AFM. There appears to be some sort of peaks (white spots) across the surface. These are most visible in the lower right corner of the image. The edges of what appear to be atomic planes seem smudged and do not seem to be well-defined. Roughness measurements were made and are presented in table 5.1. The substrate appears to be at a higher position in the upper left corner, indicating a layered structure, with the lower right part of the image being the lowest positioned STO layer in the image with several layers on top of it. Inclination of the surface was measured in Gwyddion to be 0.2°.

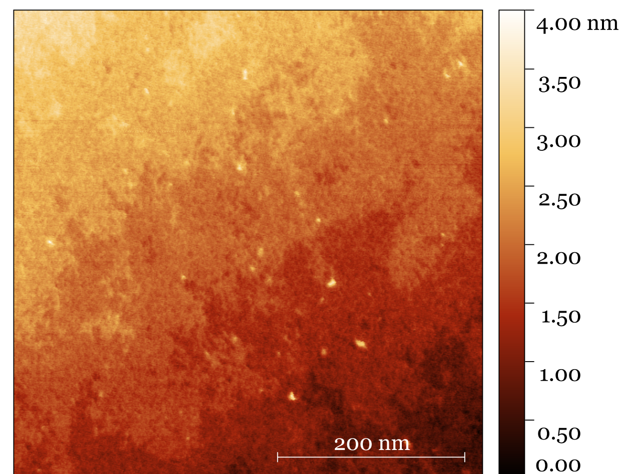

Figure 5.2: 500 nm^2 AFM image of a STO substrate treated with acetone and isopropanol

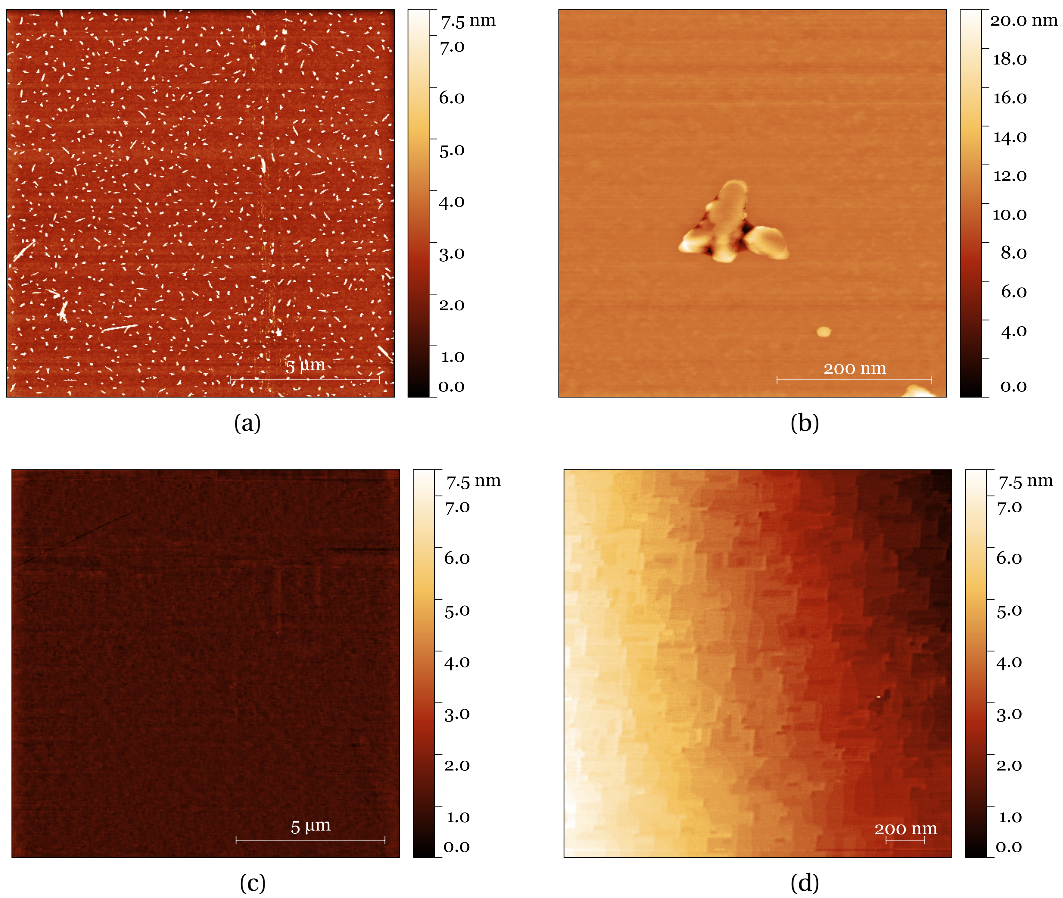

Figure 5.1: Images of untreated STO substrates. (a) (13 µm^2) and (b) (500 nm^2) are taken straight after an ultrasonic DI water bath, while (c) (13 µm^2) and (d) (2 µm^2) are taken after the substrates had been kept in air for six weeks.

5.1.1.3 Weak Waterleached Substrates

An AFM image of a substrate that was prepared using the weak waterleaching method is presented in figure 5.3. In the upper left corner of the image there appears to be a very tall structure of some sort. The rest of the surface appears to be composed of different layers of STO, as colours are not gradients, but well-defined and have sharp shifts from one area to the next. Gwyddion gives a range in altitude, from the lowest part on the substrate to the highest, of 2.733 nm. Small islands and holes appear across the largest layer on the substrate, but there is a tendency of the upper left part of the image having a larger amount of high layers than the opposite side, as if the whole surface is slanting, however, using Gwyddion gives a slope angle of 0°. The features do not appear to be very well organized and resemble step bunching. The roughness measurement from Gwyddion is presented in table 5.1.

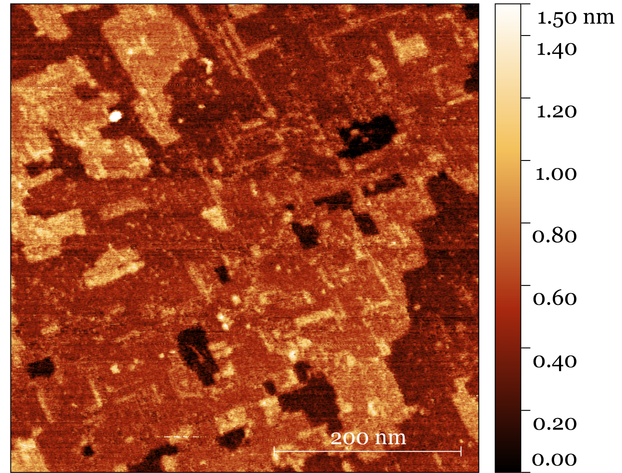

Figure 5.3: 500 nm^2 AFM image of a STO substrate treated with heat annealing and ultrasound DI water bath one time.

5.1.1.4 Waterleached Substrates

The larger part of the AFM imaging was performed on a substrate that had been waterleached, as described in section 4.1.1. This section presents AFM images of the substrates straight after, one week after, two weeks after, three weeks after, and six weeks after waterleaching. It is important to keep in mind that the substrates imaged straight after preparation and after six weeks are not the same substrates as the ones imaged after one, two and three weeks, as mentioned in 4.1.1. Roughness parameters (R_a), as estimated by Gwyddion, are shown in table 5.2.

Table 5.2: Roughness of STO substrates prepared by waterleaching as time progresses

Weeks after waterleach	Roughness[pm]
0	74.6
1	64.5
2	90.7
3	123.5
6	99.4

Figure 5.4a shows the first imaging of a newly prepared STO substrate. Layers are lying on top of other layers, and the entire image has a height difference of 8.209 nm according to Gwyddion. There are 39 distinct planes visible ranging from the high left to the lower right corner. The inclination was measured in Gwyddion to be 0.2°. The planes have well-defined

edges and there are few visible holes in them. There is however one in the lower right corner. There are also a few white specks on the surface, representing small spikes or contaminants. Figure 5.4c demonstrates a line scan over the line shown in figure 5.4b, from which the step height of the STO substrate was calculated. The result was a step height of (3.5±0.1) Å.

The roughness of the substrate was measured one week after the preparation, on the area indicated in figure 5.5a. The inclination of the entire sample was given by Gwyddion to be 0.1°. A line scan (see figures 5.5b and 5.5c) let us estimate the plane step height, which was calculated to be (2.2±0.5) Å.

After two weeks, the substrate was once again imaged using AFM, and the inclination of the image was given to be 0° (see figure 5.7b). The edges of the planes seem relatively well-defined. The number of planes in each image ranges from 15(a) to 18(c).

The AFM images taken after three weeks are shown in figure 5.8. The area from where the roughness was estimated is shown in figure 5.8b. The inclination over the entire substrate surface was estimated in Gwyddion to be 0.1°. Figure 5.8a seems to have bright specks scattered at the lower part of the image, possibly showing some form of contamination.

A 2 µm^2 AFM image of a waterleached substrate six weeks after water leaching is shown in figure 5.9. The inclination was found to be 0.1°. The substrate does not seem to have impurities, of any significance, as these would most likely appear as brighter spots.

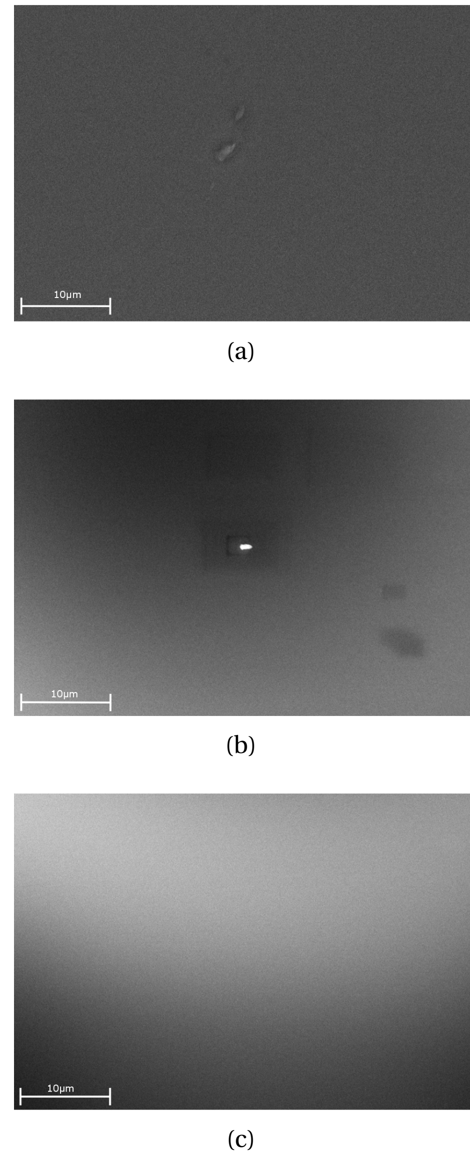

Figure 5.6: SEM images of the surface of the untreated (a), new (b) and old (c) substrates. Particles appears on both (a) and (b). Dark spots in (b) were created by the SEM instrument.

The SEM images of both the untreated, old and new substrates are shown in figure 5.6. For the most part, the surfaces appear as flat and uniform, but small particles could be seen at random locations on the surface. Particles can be seen in both figure 5.6a and 5.6b (for more images of particles, see appendix A). The dark spots visible in the lower right corner of figure 5.6b and surrounding the particle are created by the incident electron beam from the instrument and are not to be considered as a part of the substrate. The colour gradient in figure 5.6c is due to the instrument and not a real effect of the substrate. Moving the SEM signal further down toward the darker area yielded an identical image, meaning that the substrate had a relatively uniform surface in this area, and this colour effect was not a surface feature.

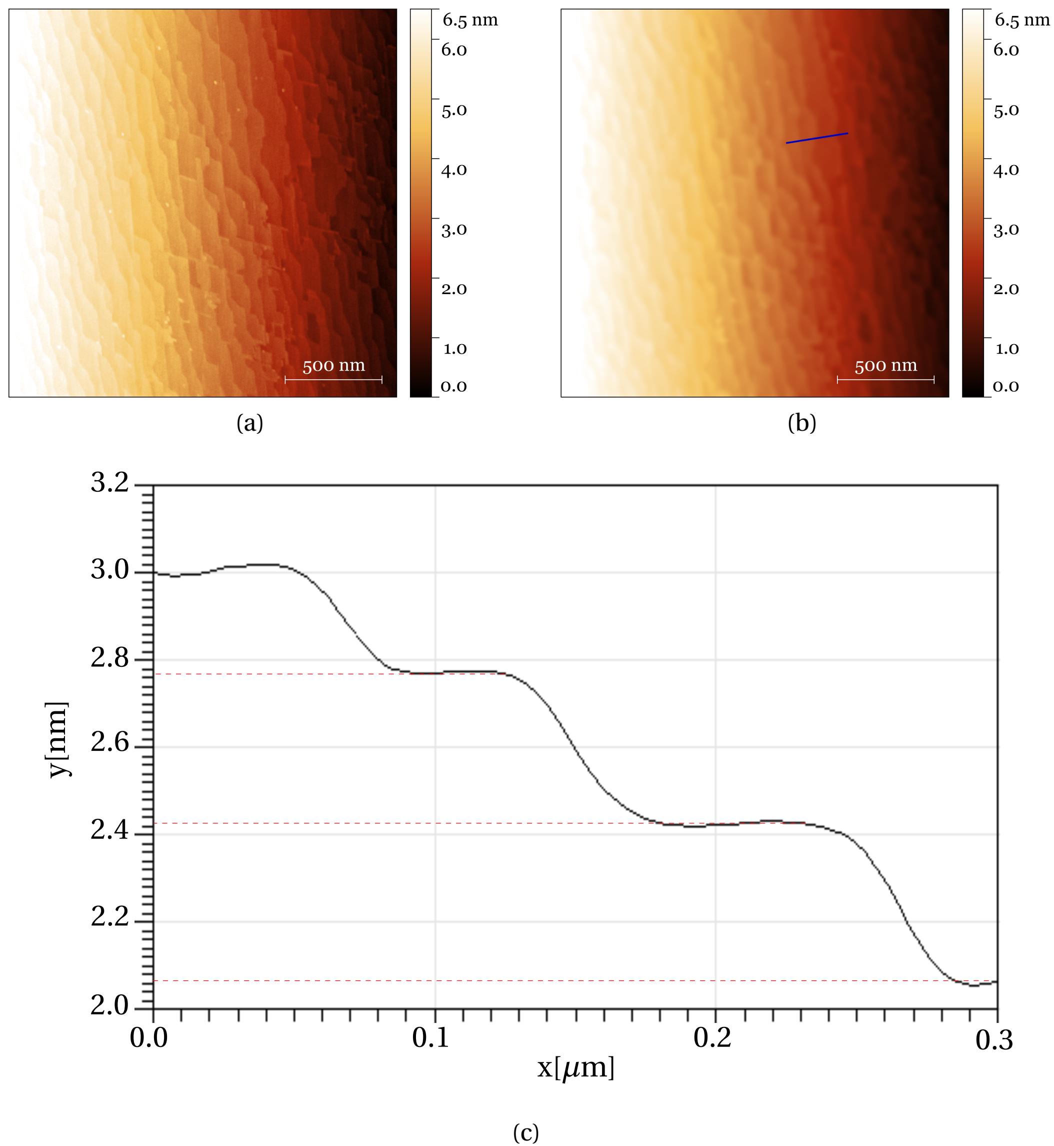

(c)

Figure 5.4: The first AFM image taken of our waterleached substrates, measuring $2\,\mu m^2$ Planes with relatively well-defined edges are lying on top of one another. (a) shows the substrate one week after waterleaching. The blue square indicates the area from where Gwyddion calculated the roughness value. (b) has been subject to basic filters (see section 4.3.1.1) and the blue line indicates the line scan shown in figure (c). The red lines in (c) were created to calculate the step height of the planes.

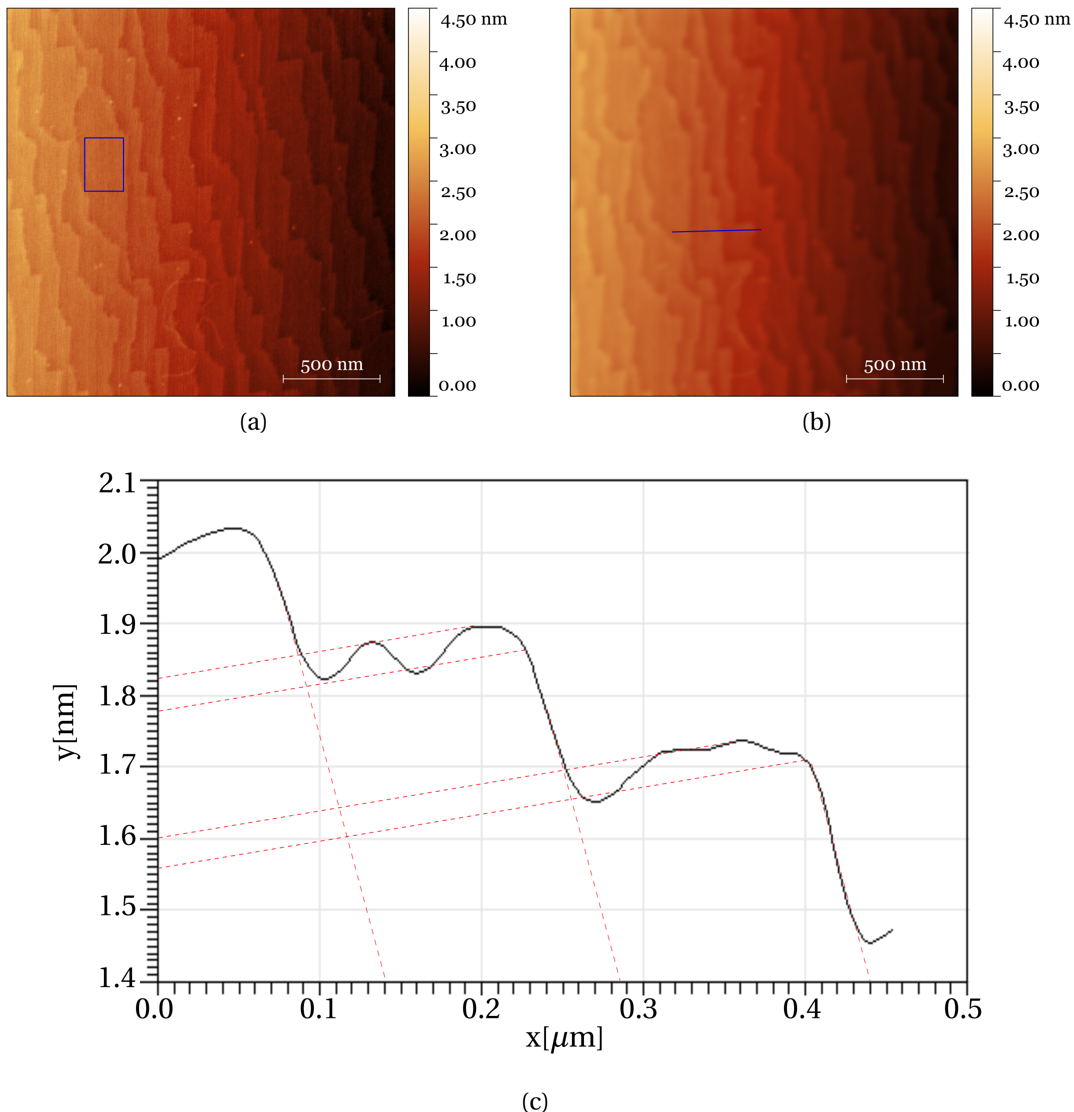

Figure 5.5: $2\,\mu m^2$ AFM image taken of a waterleached substrate one week after water leaching. Planes with relatively well-defined edges are lying on top of one another. (a) shows the substrate one week after waterleaching. The blue square indicates the area from where Gwyddion calculated the roughness value. (b) has been subject to basic filters (see section 4.3.1.1) and the blue line indicates the line scan shown in figure (c). The red lines in (c) were created to calculate the step height of the planes.

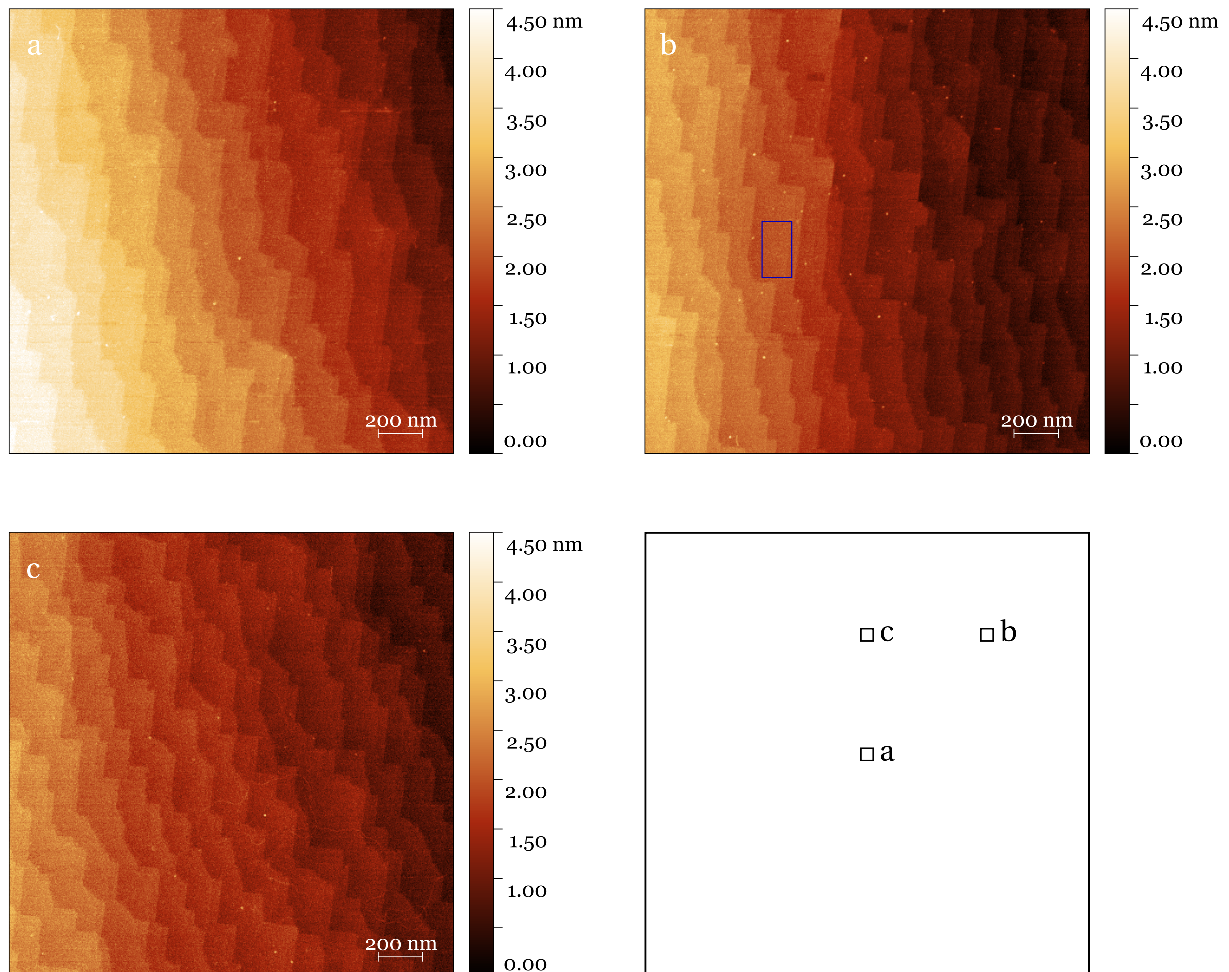

Figure 5.7: (a), (b) and (c) are 2 μm^2 AFM images at three different locations of a STO substrate, two weeks after water leaching. The location of the images is indicated in the schematic of the 1 cm^2 STO substrate in (d). The indicated locations(squares) are not to scale and the position is only for indicative purposes as there was no positioning registration of the AFM cantilever on the substrate.

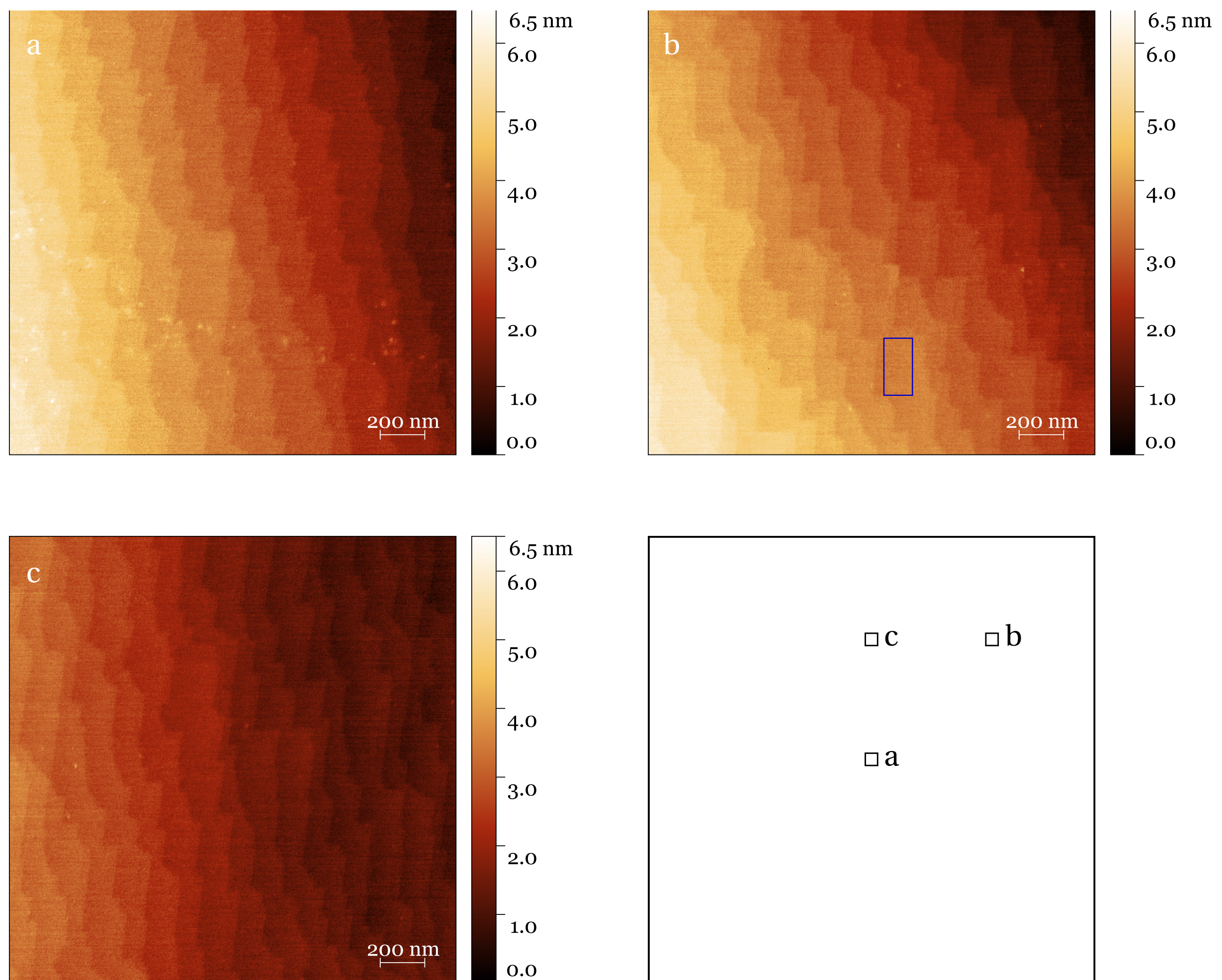

Figure 5.8: (a), (b) and (c) are 2 μm^2 AFM images at three different locations of a STO substrate, three weeks after water leaching. The location of the images is indicated in the schematic of the 1 cm^2 STO substrate in (d). The indicated locations(squares) are not to scale and the position is only for indicative purposes as there was no positioning registration of the AFM cantilever on the substrate.

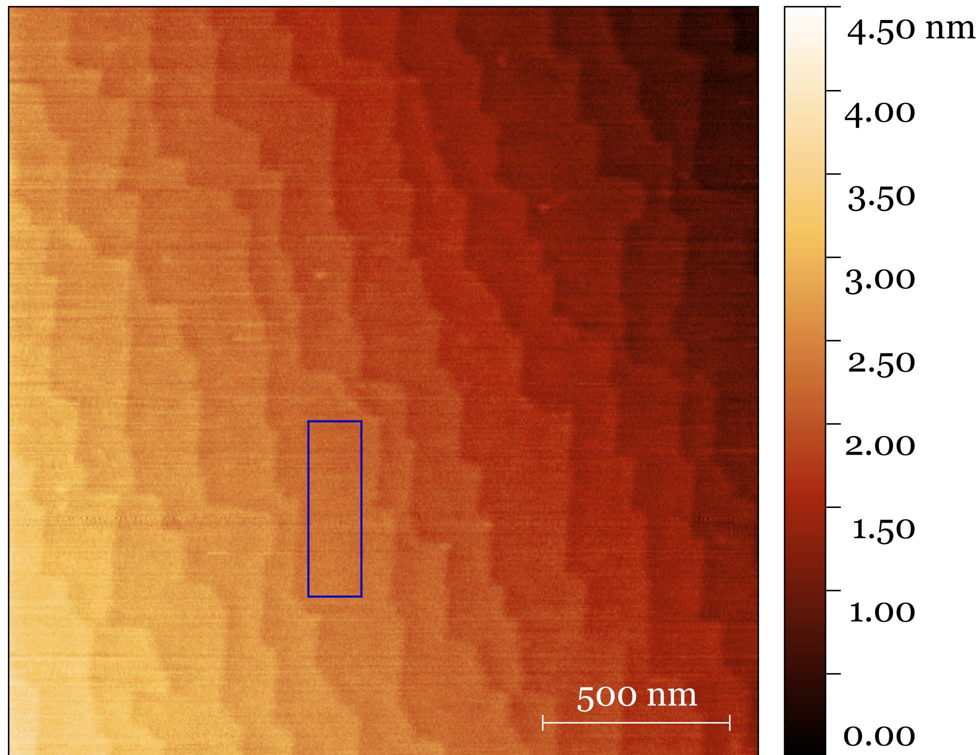

Figure 5.9: 2 μm^2 image of a STO substrate six weeks after waterleaching. A blue square indicates the area from where the roughness was estimated.

5.1.2 Surface Composition of Untreated Substrates

Survey scans of untreated, new and old substrates are shown in figure 5.11. Figure 5.11a shows the first three survey scans in the same plot, all performed on the old substrate. The survey scans performed on new (see figure 5.11b) and untreated (see figure 5.11c) were done with a higher anode current and energy, to increase the output signal strength. Both figures have an overlay of all the three scans. Figure 5.11d shows all of the survey scans combined in the same figure. Remember that the CPS shift is due to the factors mentioned in section 4.3.2. All peaks were located using the NIST database [41].

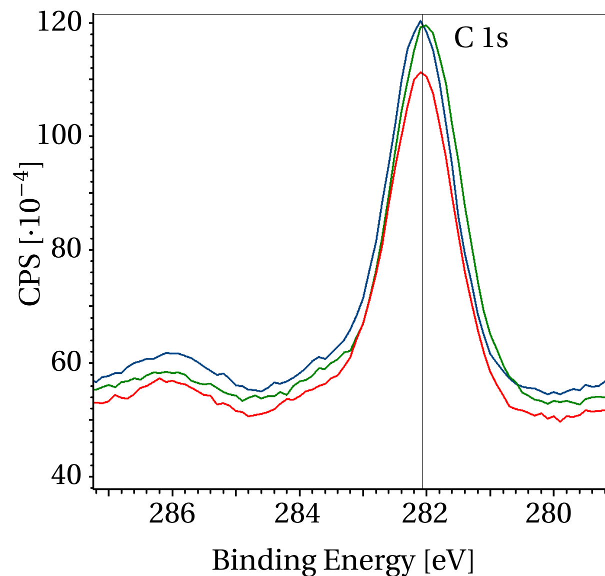

Figure 5.10: Carbon peaks on the old, new and untreated substrates. The vertical line indicates the approximate centre of all the peaks. Blue, green and red lines represent untreated, new and old substrates, respectively.

The surveys taken at the adventitious carbon peaks of each sample is shown in figure 5.10. They were all centred at the same binding energy, of approximately 182 eV. By using this value, the entire spectrum in all the

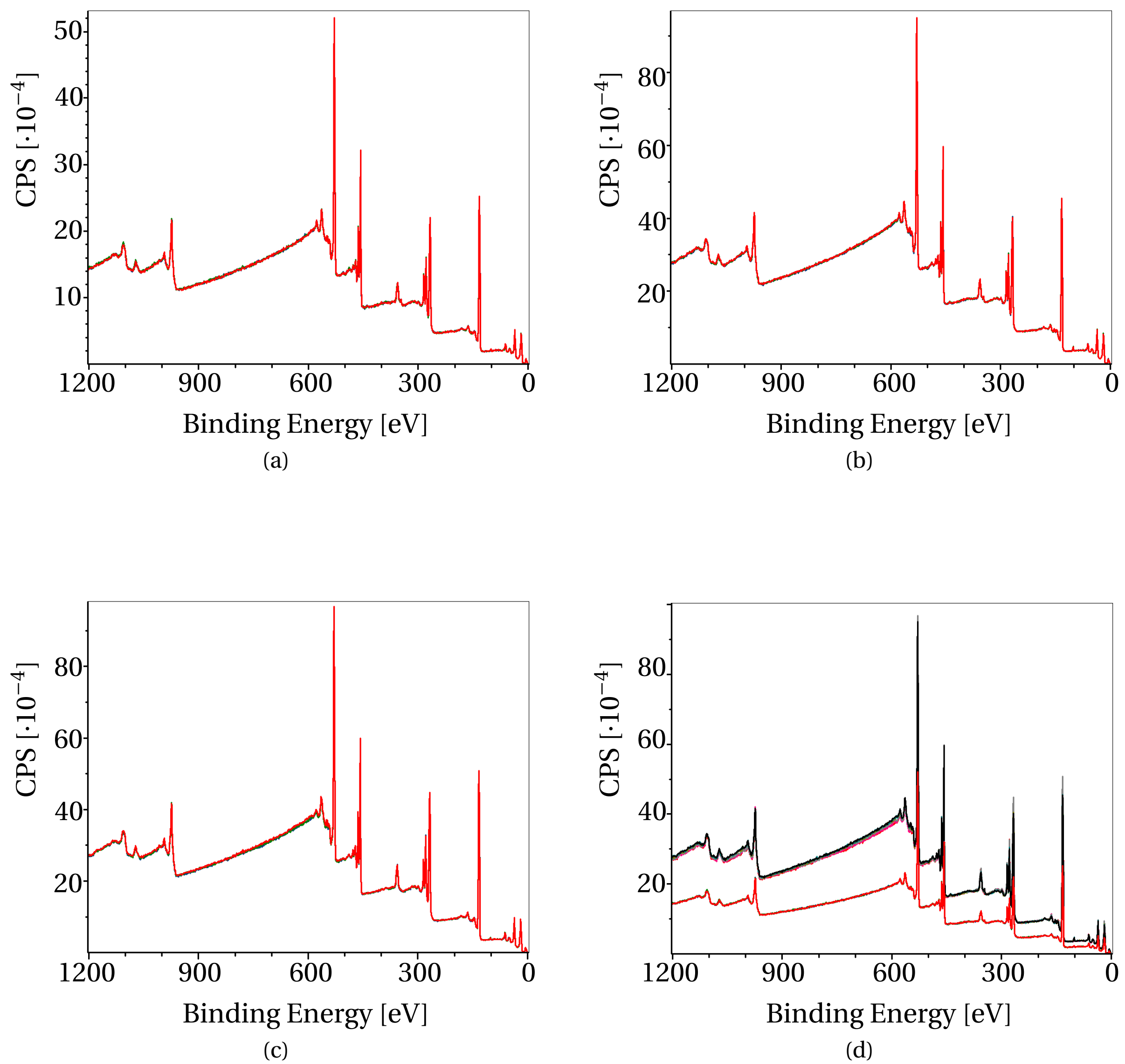

Figure 5.11: (a), (b) and (c) shows XPS survey scans performed on the old, new and untreated substrates, respectively. Each substrate was characterized by three survey scans, which have been combined in all of the first three figures. (d) shows all the survey scans combined in the same figure.

figures in this entire section was shifted by 184.8 − 182 = 2.4 eV, as 184.8 eV is the binding energy for adventitious carbon. The scan also indicated that there was less carbon present at the old substrate than the other two, which were almost equal at the maximum peak.

The XPS spectrum of strontium on the untreated, new and old substrates is shown in figure 5.12a. The most intense measurement was made from the untreated substrate, while both the new and old are as good as overlapping, at a lower CPS. Vertical lines indicating the values from CASA for Sr $3d_{3/2}$ (135 eV) and Sr 3d $_{5/2}$(133 eV) are plotted as well. All the plots have been shifted by the results made from the carbon peak survey. The leftmost peaks in our scan are located at approximately (134.50±0.05) eV, whereas the rightmost are located at approximately (132.65±0.05) eV, giving a separation of (1.8±0.1) eV. The last of these values fit well with the given value for $SrTiO_3$ from [41], while the leftmost peaks gives most likely is a strontium peak, according to [41].

XPS around the oxygen peak, as well as CASA's value for oxygen 1s (532 eV), is shown in figure 5.12b. The plot has been shifted by the amount specified by the adventitious carbon peaks. The maximum intensity peak of all plots appear to be at approximately (529.4±0.1) eV, corresponding to both TiO_2 (with binding energy of 529.4 eV) and STO (with binding energy of 129.3 eV). Yet again, there is a stronger CPS for the untreated than on the new and old substrates. The small variation around the left shoulder of the maximum peaks indicate a presence of other species of oxygen. At the lower left shoulder, the highest CPS comes from the new substrate, followed by the untreated and old. Fitting a curve to the scan data gives a maxima for the lower shoulder at (531.4±0.2) eV corresponding quite well to TiO_2 at 531.2 eV.

The titanium peak XPS spectrum is shown in figure 5.12c along with vertical lines representing CASA library values for both Ti $2p_{1/2}$ (461 eV) and Ti $2p_{3/2}$ (455 eV). All the scans have been shifted by the adventitious carbon calibration parameters. The maximum intensity peak of what appears to be a doublet, appear to be at approximately (458.30±0.15) eV, corresponding to TiO_2, while the lower peaks appears at approximately (464.1±0.3) eV, also corresponding to TiO_2. This figure also shows the untreated substrate as the one with the highest CPS both at the higher and the lower peak.

5.1.3 Bulk and Surface Composition

For the most part, the untreated, new and old substrates appeared flat when doing SEM imaging, like the image of the old substrate, shown in figure 5.6c. There were, however, a few particles scattered across the surface, as seen in the middle of figure 5.6a and 5.6b, ranging in size from 1 µm to 10 µm. As apparent in figure 5.13 and 5.14, the untreated, new and old substrates were all dominated by strontium, followed by titanium and oxygen. Surprisingly, there was registered small amounts of nickel (see figure 5.13) at all of the substrates, as well as small amounts of aluminium at both the untreated and old substrates (see figure 5.13a and 5.13c). Carbon was seemingly only found at the untreated substrate.

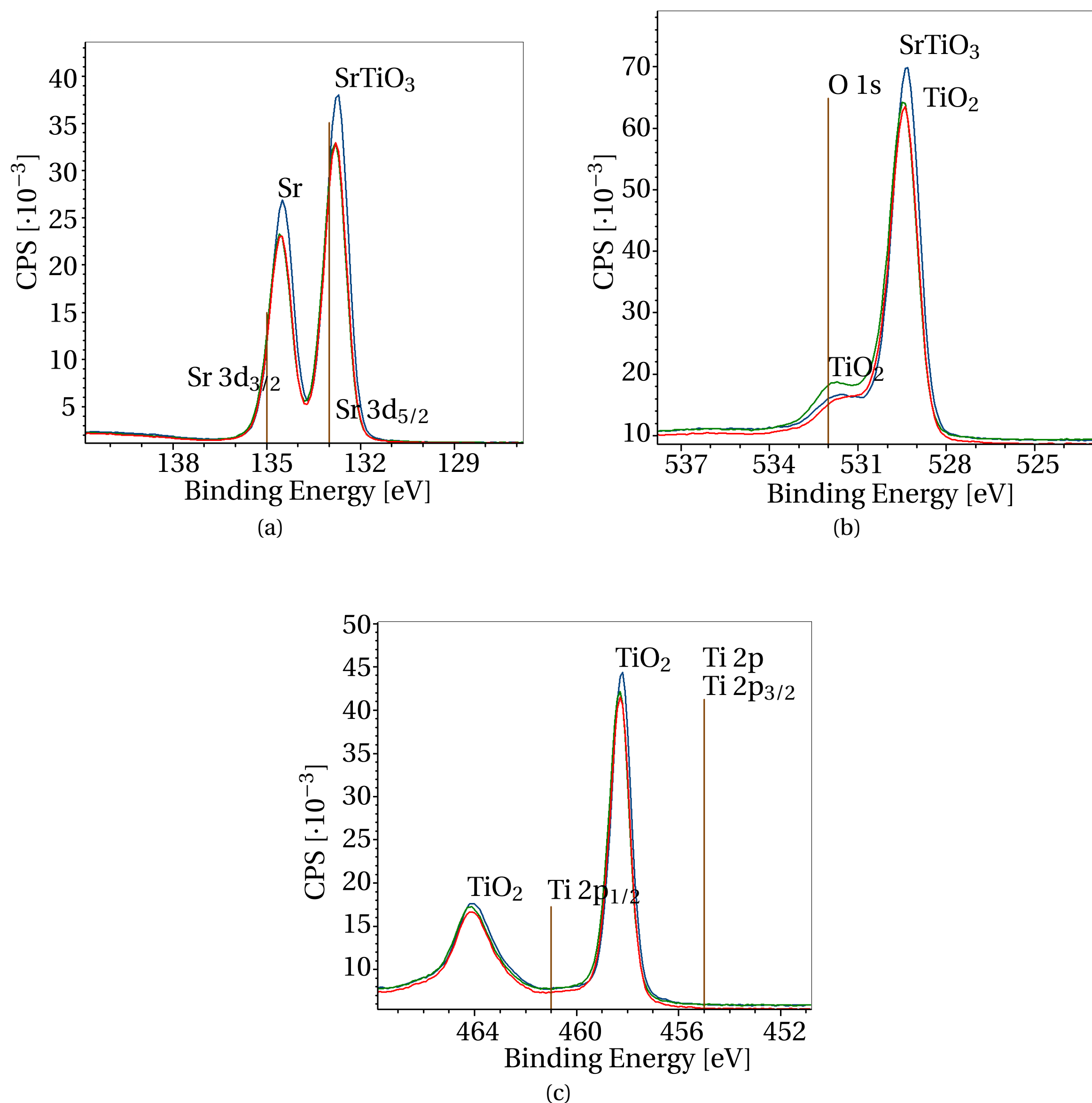

Figure 5.12: Detailed XPS scans of strontium doublet (a) (vertical lines at Sr $3d_{3/2}$ (135 eV) and Sr 3d $_{5/2}$ (133 eV)), oxygen doublet (b) (vertical line at 532 eV) and titanium doublet (c) (vertical lines at Ti $2p_{1/2}$ (461 eV) and Ti $2p_{3/2}$ (455 eV) on untreated, new and old substrates. Vertical lines were created using values from the CASA library. The blue, green and red lines in each plot represents untreated, new and old substrates respectively.

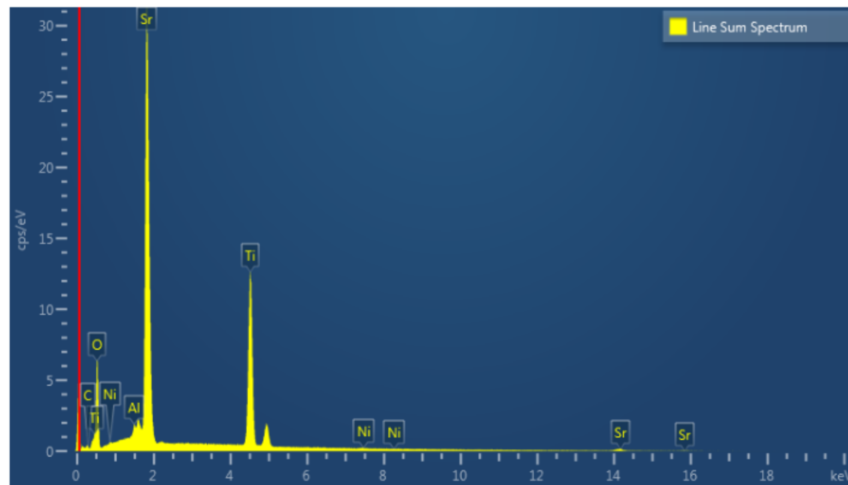

(a)

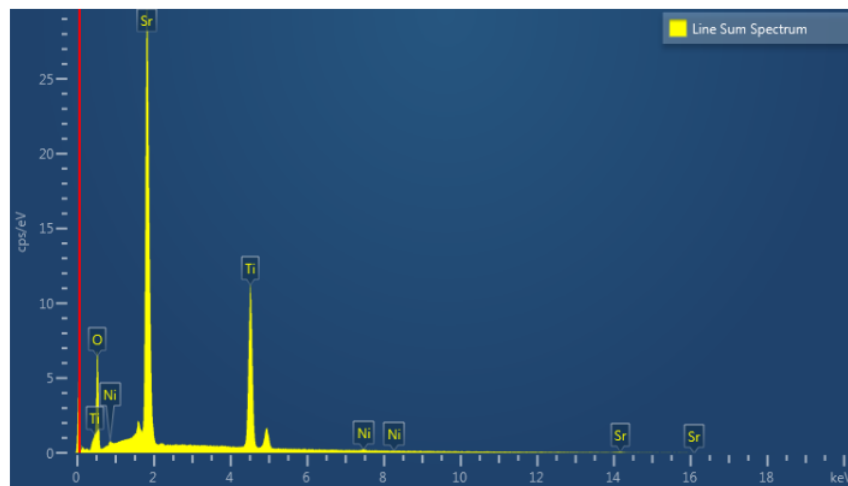

(b)

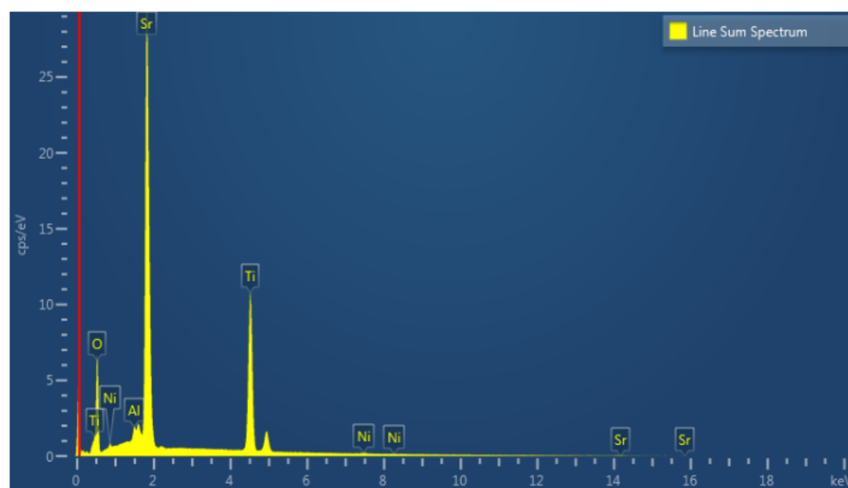

(c)

Figure 5.13: EDS spectra of a line scan on the untreated (a), new (b) and old (c) substrates.

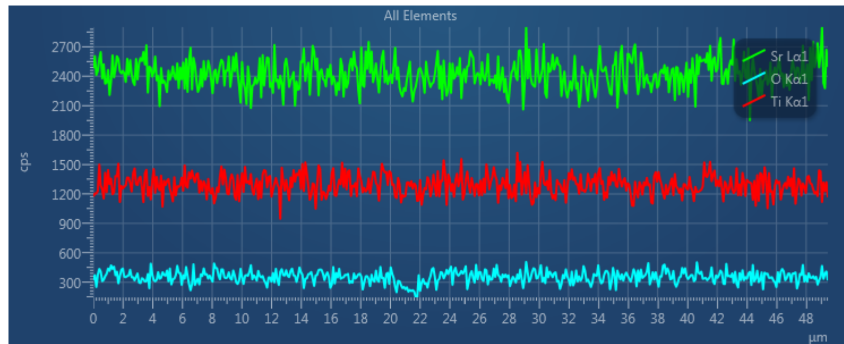

(a)

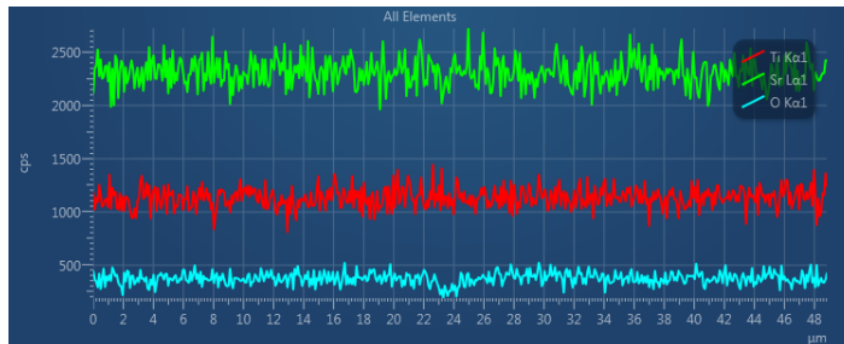

(b)

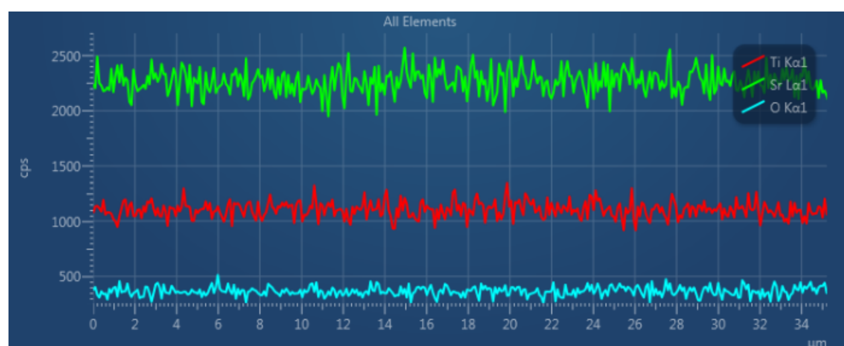

(c)

Figure 5.14: EDS line scans of the untreated (a), new (b) and old (c) substrates, green indicating strontium, red indicating titanium and blue indicating oxygen

5.2 Thin Film Studies

The different thin films had some limitations in the way they could be characterized. Profilometer scans to determine thin film thickness could only be performed on the substrates from the PLD experiments, because these substrates were partly covered during the deposition and the EBPVD deposited thin films were not. XRD was performed only on the thin films, and not the substrate, as these were made from a single-crystal. XPS was performed on TiO_2 thin films deposited by both PLD and EBPVD on newly prepared STO substrates, in addition to the PLD deposition on the Si substrate. The results from all of this, in addition to EDS line scans over all seven thin films, is presented in the following section.

5.2.1 Deposition Rate of PLD Deposited TiO_2 Thin Films

Profilometer scans were taken from all the thin films that were deposited using PLD and they can be seen in figure 5.15. The results were obtained by using the best of several scans on each substrate and were treated using the instrument software to the max of its capacity. Dashed lines were added later, to give a pointer as to what the thickness of the thin films were. Using these values, we got measurements of the TiO_2 thin film thickness and deposition rates as shown in table 5.3.

Table 5.3: PLD deposited TiO_2 thin film thickness's and calculated deposition rates.

Substrate	Thickness[nm]	Deposition rate [pm/pulse]
Untreated	110	4.58
New	128	5.33
Old	145	6.04
Si	125	5.21

5.2.2 Surface Composition

X-ray spectroscopy was performed on TiO_2 thin films deposited on newly treated STO substrates by both PLD and electron beam physical vapour deposition (EBPVD), as well as a silicon substrate. Adventitious carbon peaks were located and the spectra were moved by the corresponding values. Both PLD deposited thin films showed similar characteristics, while the EBPVD deposition was somewhat different. Three survey scans were taken over the substrates, and all peaks of interest were studied further. The resulting spectra can be seen in figure 5.16.

Figure 5.16a shows detailed XPS scans of the oxygen doublet, with a vertical line at O 1s (532 eV). The PLD deposited thin films shared similar characteristics, with the largest peak at (529.78±0.08) eV corresponding to TiO_2, while the EBPVD deposited thin film had the largest peak at (530.15±0.01) eV, also corresponding to TiO_2. The lower peak, appearing as a shoulder on the left side of the large peaks were found to also correspond to TiO_2.

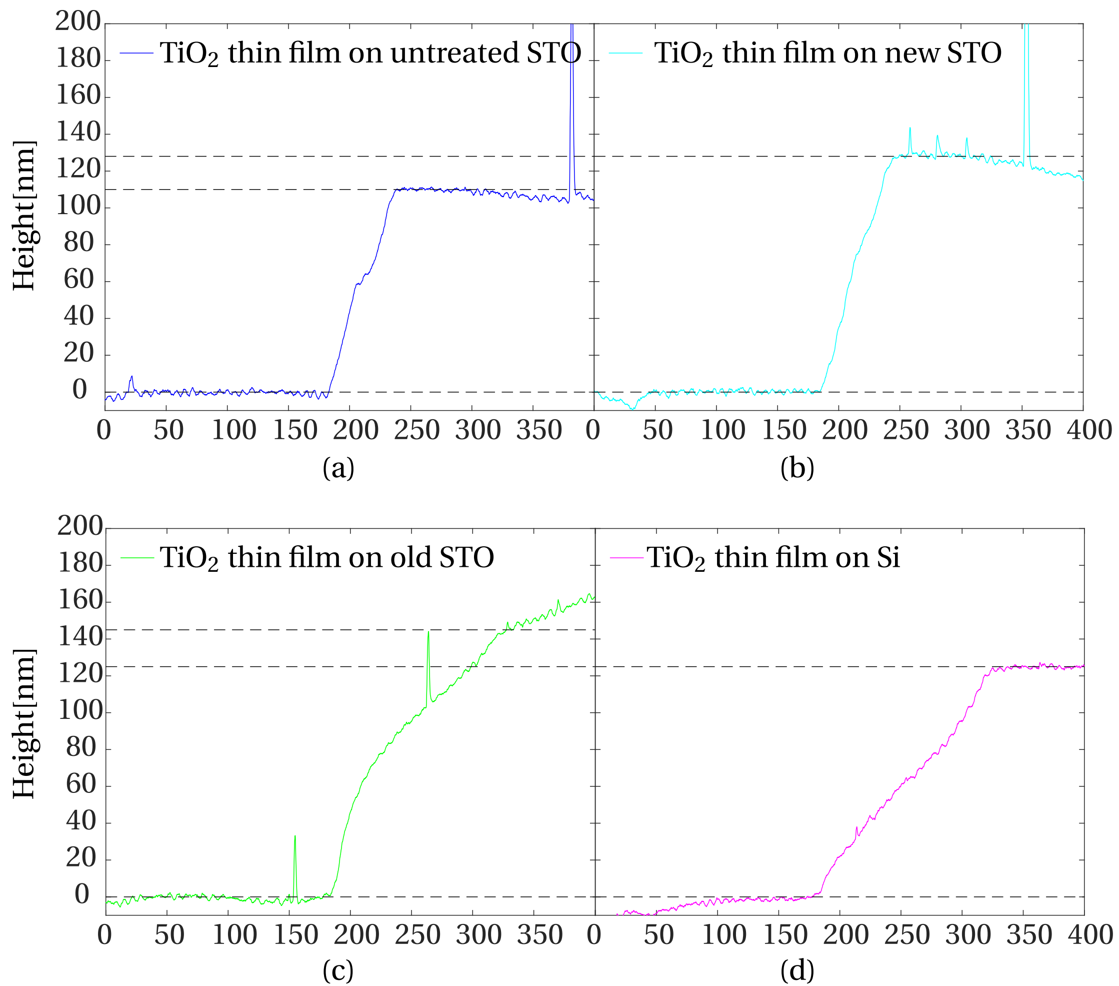

Figure 5.15: (a), (b) and (c) shows profilometer scans over the edge of the TiO_2 thin films that were deposited by PLD on untreated, new and old substrates, respectively. (d) shows a profilometer scan over the edge of the TiO_2 thin film deposited on a Si substrate in the same PLD deposition experiment. Dashed lines indicate approximate values for start and end position of height measurements.

Figure 5.16b shows the resulting spectra from our titanium doublet, with vertical lines at Ti $2p_{3/2}$ (461 eV) and Ti $2p_{5/2}$ (455 eV). All peaks were found in [41] to correspond to TiO_2.

Figure 5.16c shows the spectra for silicon, with vertical lines at Si $2p_{1/2}$ (100 eV) and Si $2p_{3/2}$/ Si 2p (99 eV). The PLD deposited thin films have a peak for silicon, which cannot be said for the EBPVD deposition, as the slightly elevated CPS values in the SiO_x/Si are within the noise region.

5.2.3 Crystallinity

All seven thin films were characterized using gracing incidence X-ray diffraction (GI-XRD). The data from the thin films deposited using PLD on STO and silicon substrates, are shown in figure 5.17, together with table values for the best crystal fit found by the software. The measurements seem quite noisy, even though they have been subjected to smoothing functions, and so, the best matching of the scans with table values were 57 %, 44 % and 57 % for the untreated, new and old substrate, respectively, while the thin film on the Si substrate had a match of 59 % with monoclinic Ti_3O_5. The crystal matching was performed before the curves had been smoothed, as the smoothing was only done to make measurements easier to read in the figure.

The thin films deposited by EBPVD see figure 5.18 had the best matches with monoclinic structures. The thin film deposited on the untreated and newly treated substrates had the best matching with monoclinic TiO_2, with matches of 91 % and 97 %, respectively. The thin film deposited on the old STO substrate had a 67 % match with monoclinic Ti_3O_5.

5.2.4 Surface Structure and Thin Film Composition

SEM images of all six TiO_2 thin films deposited on untreated, new and old substrates, are shown in figure 5.19 and 5.20 with the lines over which the EDS was performed. Most of the surfaces appeared as relatively uniform, with small particles at random locations and far in between. One such particle can be seen in figure 5.19b, another in figure 5.21a, and even more in appendix A.

The image and EDS data from the TiO_2 thin film deposited on untreated STO is shown in figure 5.21. While most of the surface of the thin film was flat and uniform, just as the background of the image in figure 5.21a, there were some particles at seemingly random intervals. These made focusing easier, and a line scan of the particle and some of the surrounding thin film is shown in figure 5.21c and 5.21d. The measurement clearly shows the presence of titanium, oxygen and strontium, but also carbon, located at the particle. An EDS measurement of carbon on the entire image can be seen in figure 5.21b and shows that the carbon is highly localized to the particle.

Figure 5.22 shows a similar particle, but at the surface of the TiO_2 thin film deposited on a new STO substrate. This particle is also, clearly made up of carbon, which can be seen from the line scan data in figure 5.22b and 5.22c).

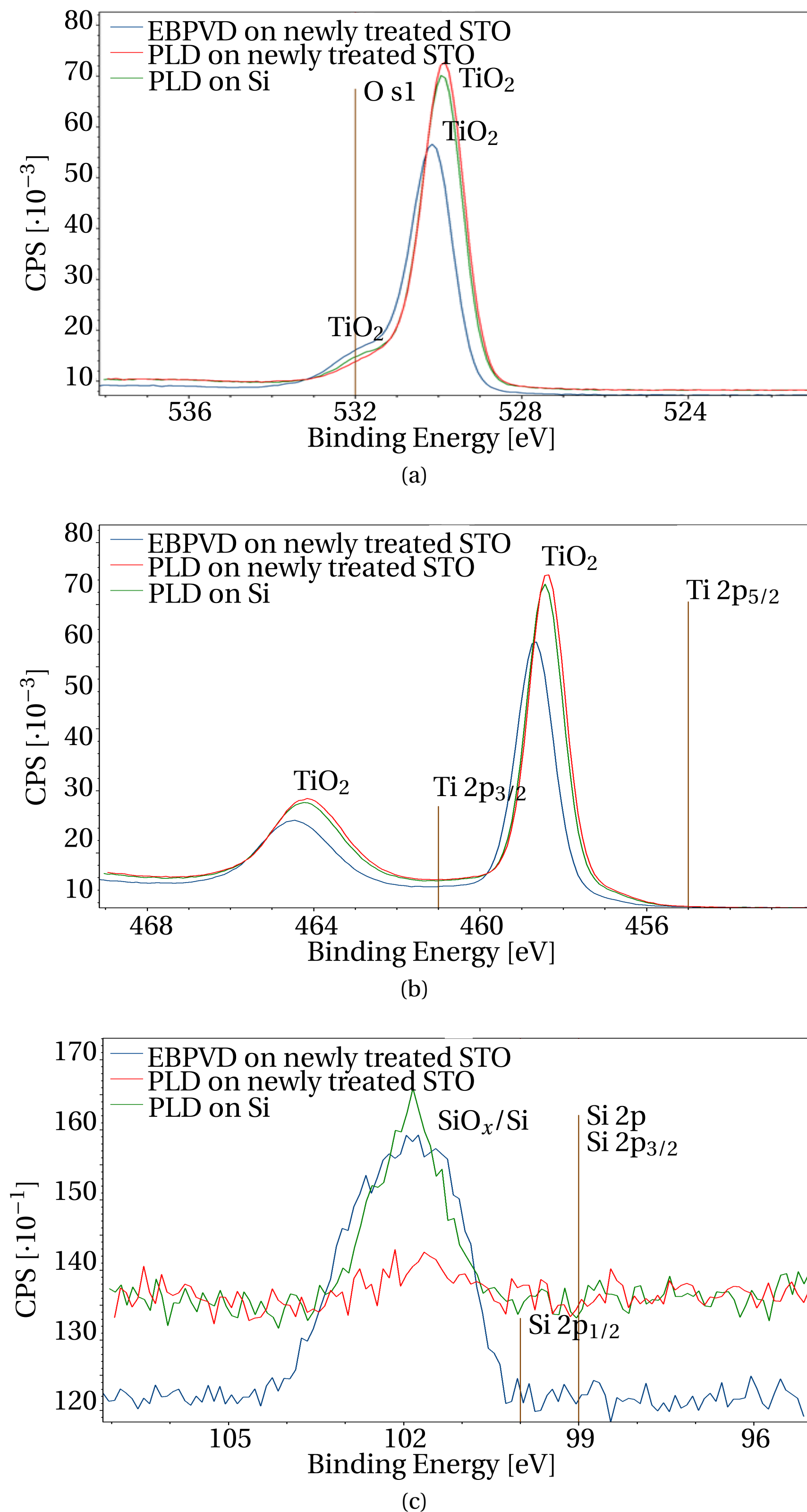

Figure 5.16: Detailed XPS scans of oxygen doublet (a), titanium doublet (b) and silicon (c) on TiO_2 thin films deposited on new STO substrates by PLD and EBPVD and on a silicon substrate by PLD. Vertical lines indicate elements from the CASA library.

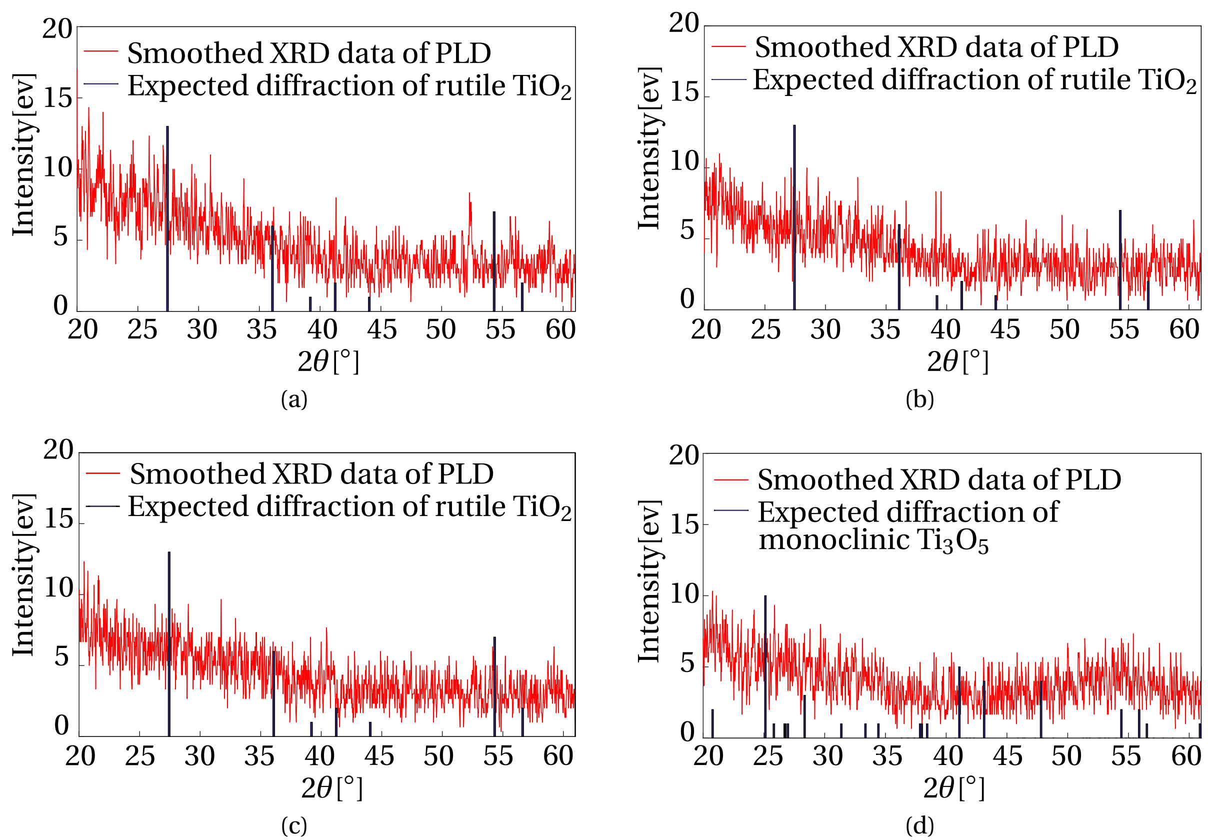

Figure 5.17: XRD measurement of a TiO_2 thin film deposited by PLD on untreated (a), new (b) and old (c) STO substrates with tabular values for rutile TiO_2 as a box plot as this was the best fit for all these thin films. (d) is the XRD measurement for a TiO_2 thin film deposited on a silicon substrate, with the best fit, of monoclinic Ti_3O_5, plotted as well.

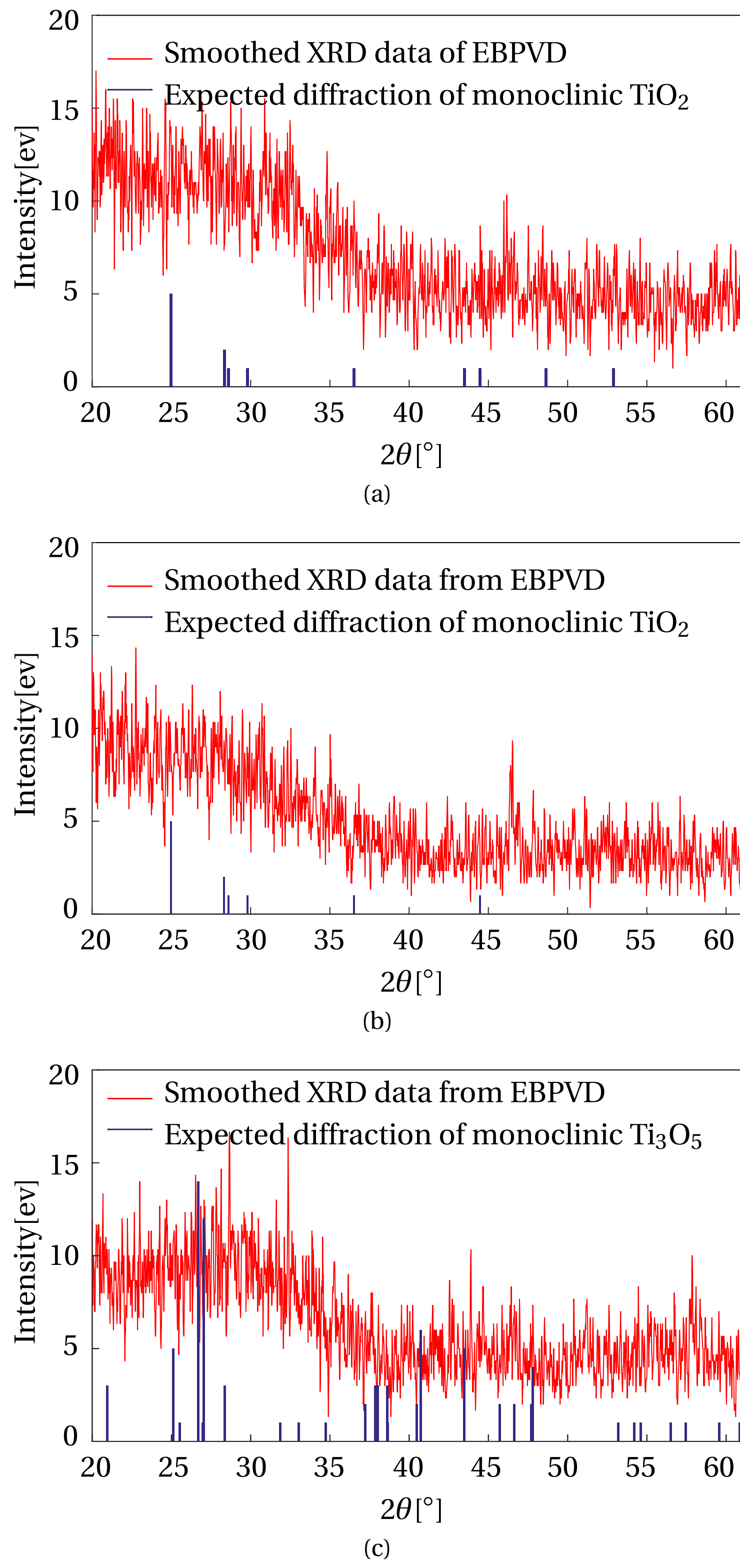

Figure 5.18: XRD measurement of a TiO_2 thin film deposited by EBPVD on an untreated (a), new (b) and old(c) substrate with tabular values for the best fitting material as a box plot. For (a) and (b) the best fit was made for monoclinic TiO_2, while for (c) it was monoclinic Ti_3O_5.

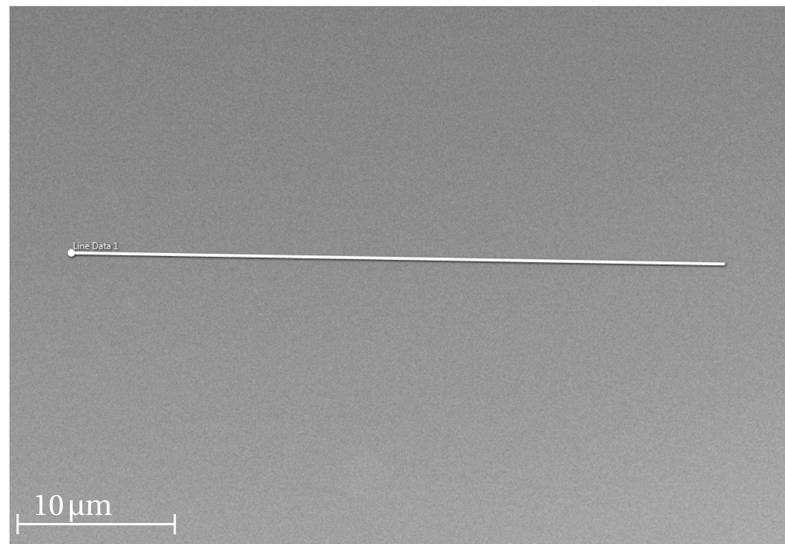

(a)

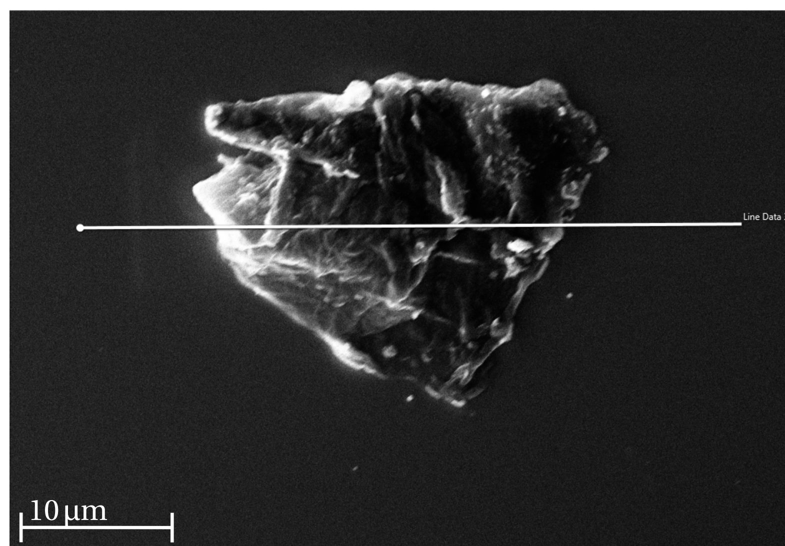

(b)

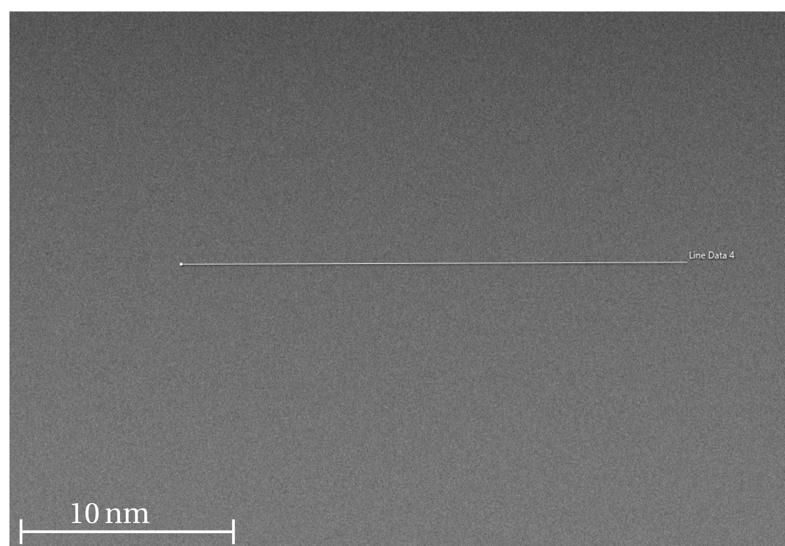

(c)

Figure 5.19: (a), (b) and (c) are SEM images of TiO_2 thin films deposited by PLD on untreated, new and old STO substrates, respectively. (b) includes a particle that was found at the surface. Lines over which EDS was performed are marked in each image.

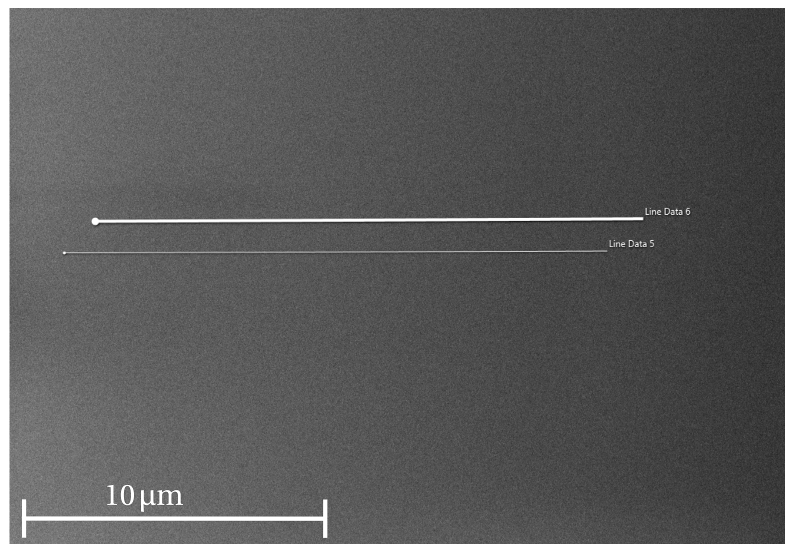

(a)

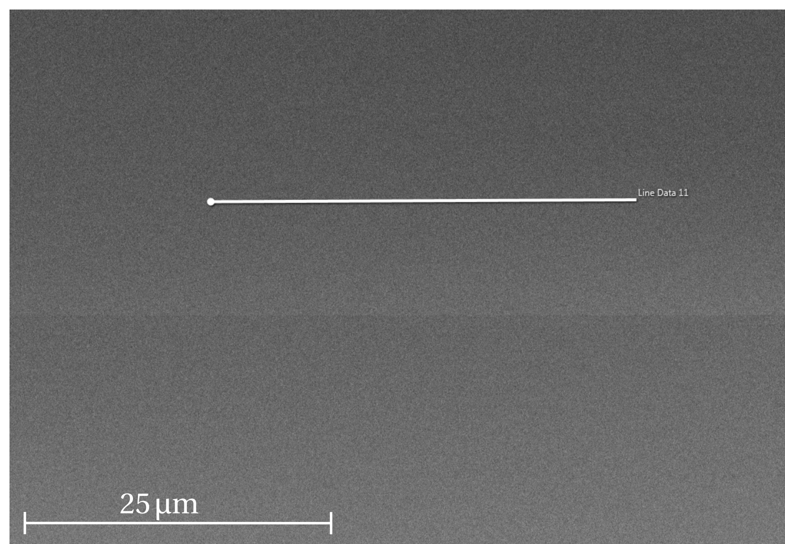

(b)

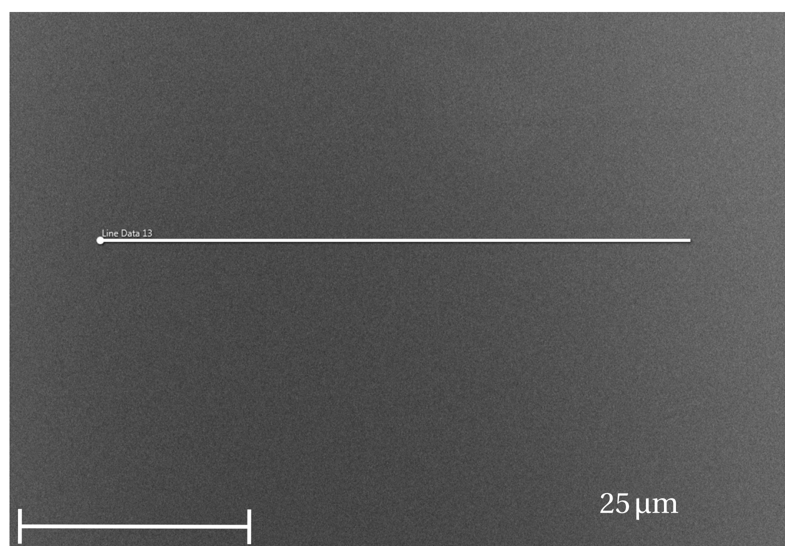

(c)

Figure 5.20: (a), (b) and (c) are SEM images of TiO_2 thin films deposited by EBPVD on untreated, new and old STO substrates, respectively. Lines over which EDS was performed are marked in each image.

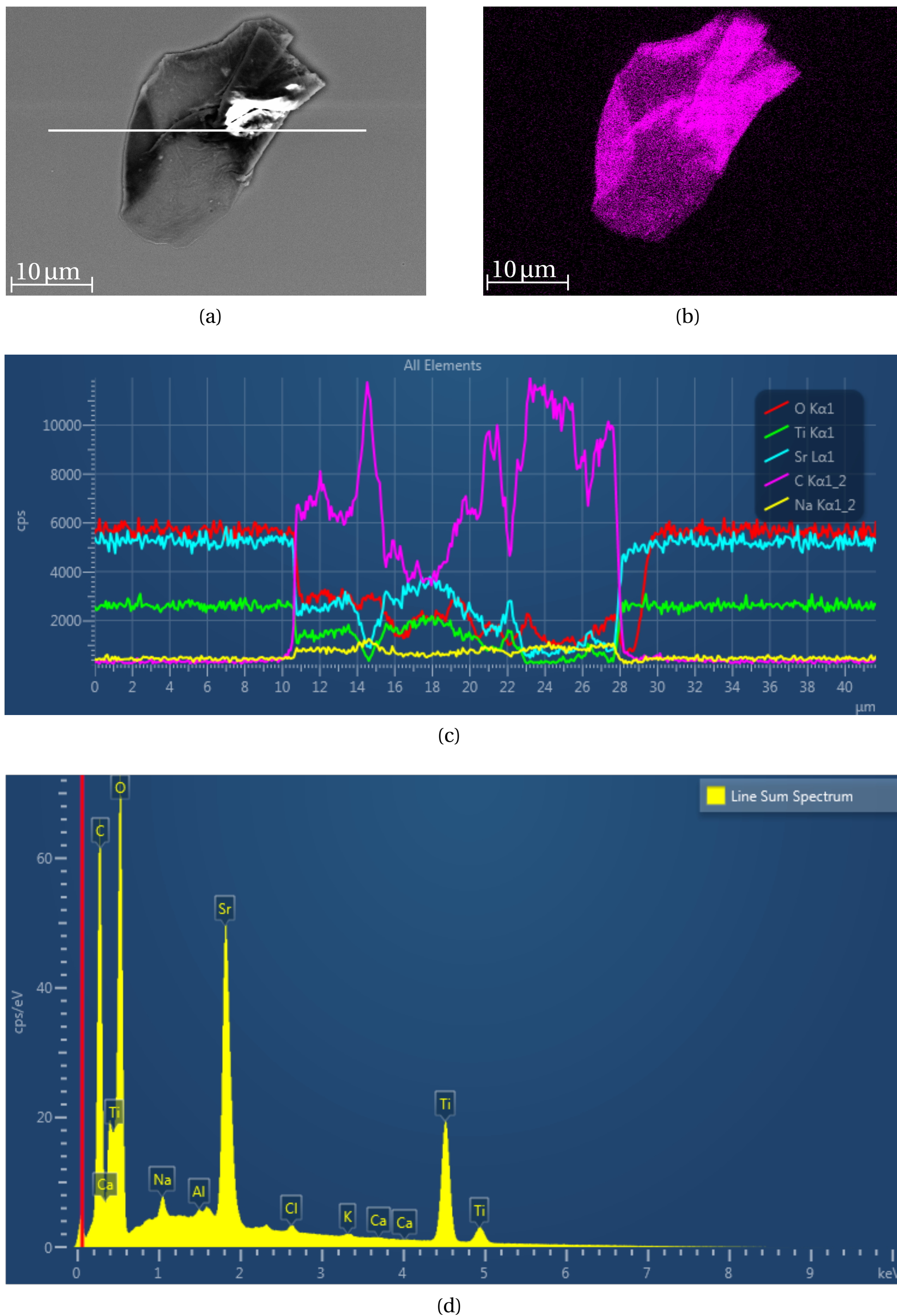

Figure 5.21: (a) shows a SEM image of a particle at the surface of a TiO_2 thin film deposited on an untreated STO substrate by PLD. (b) presents an EDS scan of carbon on this area, while line scan data is presented in (c) and (d).

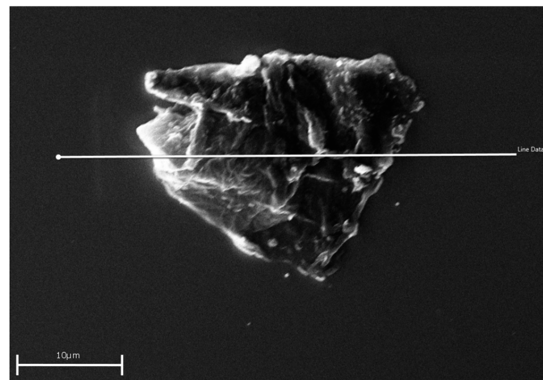

(a)

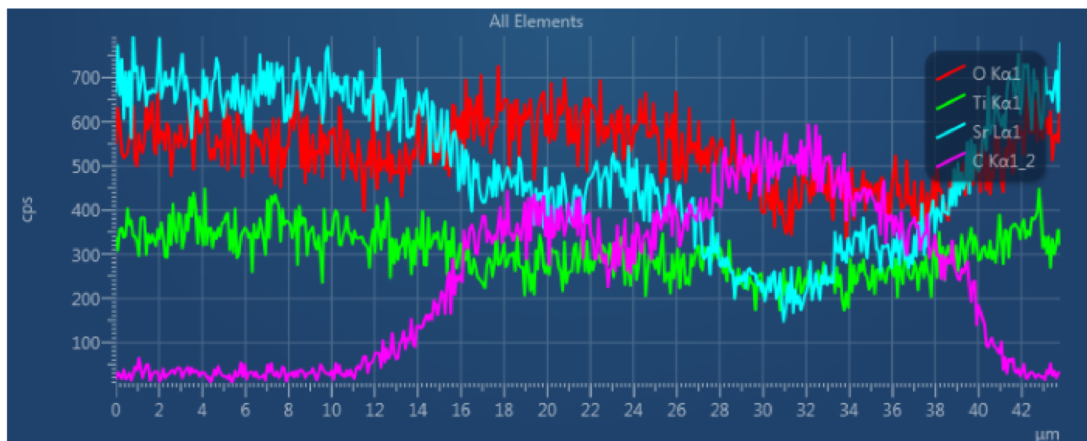

(b)

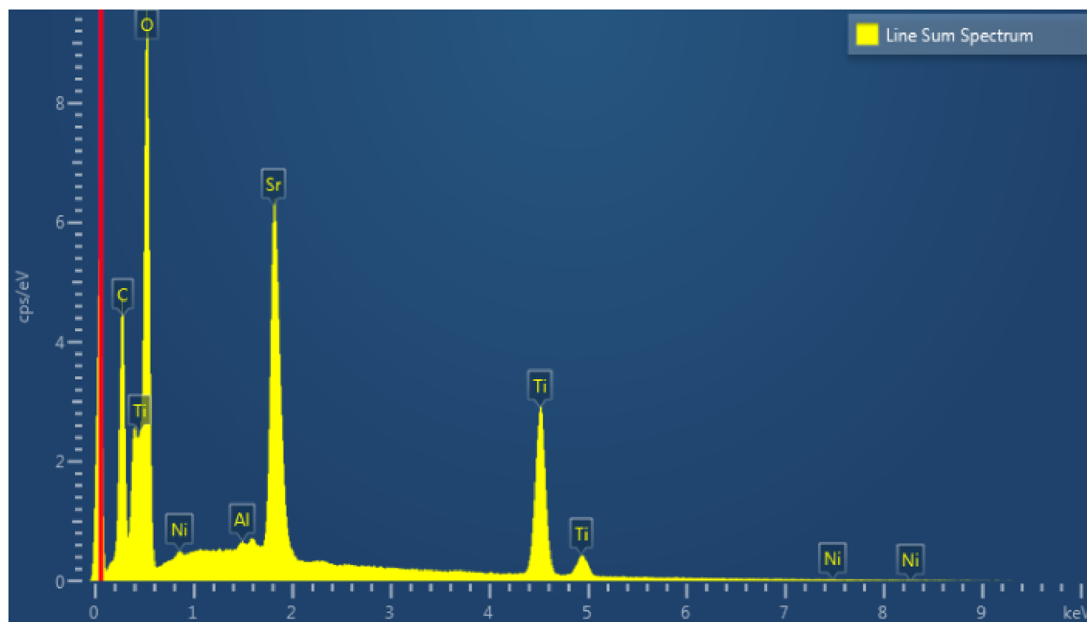

(c)

Figure 5.22: (a) is a SEM image of a particle at the surface of a TiO_2 thin film deposited on a newly waterleached STO substrate by PLD and data from an EDS line scan is presented in (b) and (c).

The EDS data from the TiO_2 thin film deposited on a silicon substrate can be seen in figure 5.23. There seems to be a very large presence of silicon compared to both titanium and oxygen at most of the thin film, except for the particle (see figure 5.23a), where titanium suddenly increases and silicon drops off.

EDS line scans of the thin films deposited by PLD on STO substrates are shown in figure 5.24. Figure 5.24b shows a scan that was performed over a particle at the sample surface, and therefore, the purple line, representing carbon, makes sudden shifts in the middle of the plot. The area outside of the most intense carbon region can, however, be compared to the other scans, as this area was outside of the carbon particle. All other line scans of the PLD deposited thin films were done at what appeared to be completely flat parts of the deposited TiO_2 thin films. In all the scans, oxygen, strontium and titanium is the most heavily represented, with carbon only appearing at thin film deposited on the new substrate, where the carbon particle is located. Strontium and oxygen appears as more abundant than titanium, bit this might be due to elemental response.

All the EBPVD deposited thin films (see figure 5.25) shows that titanium and strontium are in abundance compared to oxygen (see figures 5.25a, 5.25b and 5.25c). Carbon appears only at the EBPVD deposition on the old substrate.

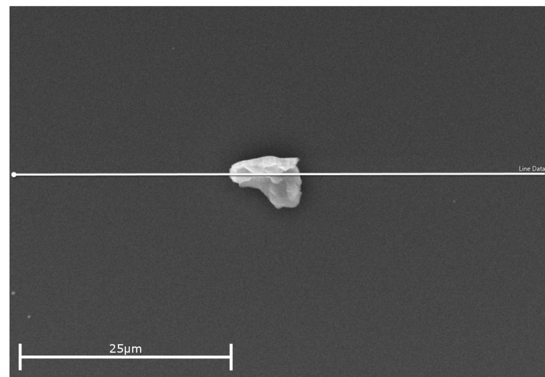

(a)

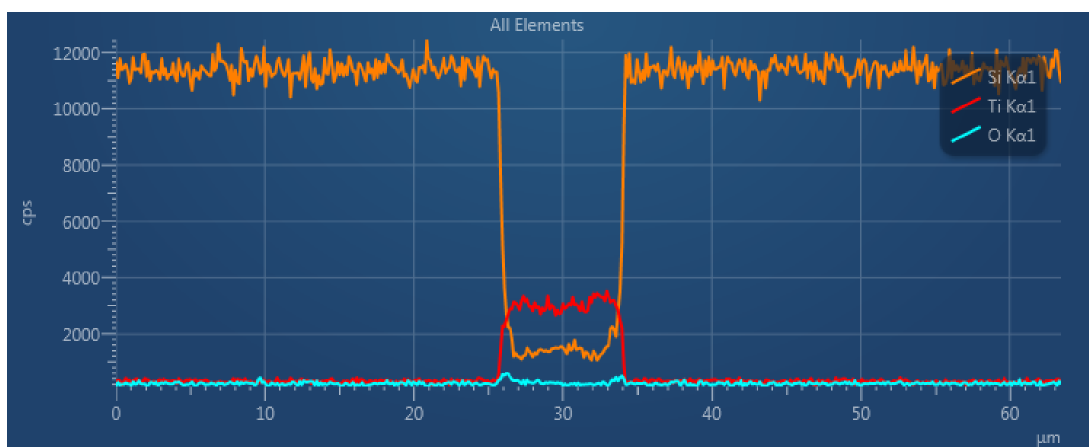

(b)

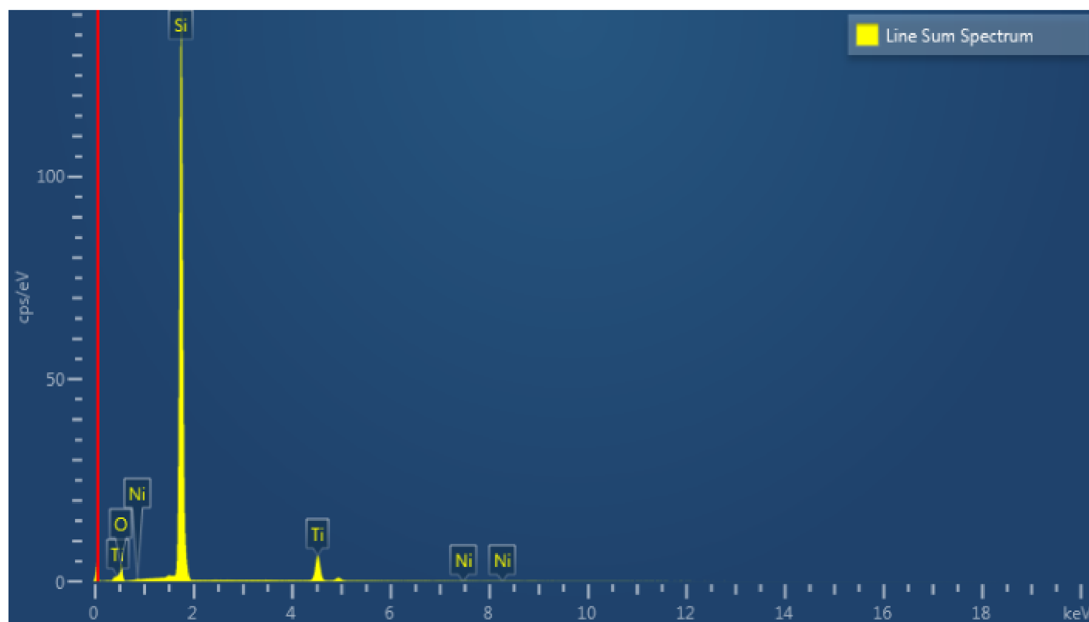

(c)

Figure 5.23: SEM image of a particle at the surface of a TiO_2 thin film deposited on a silicon substrate by PLD and data from an EDS line scan.

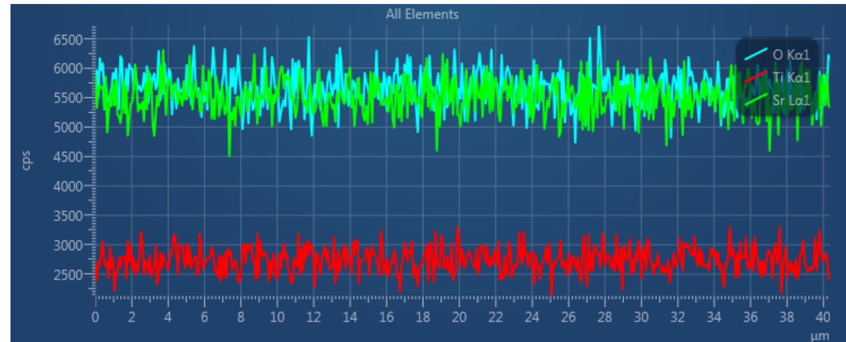

(a)

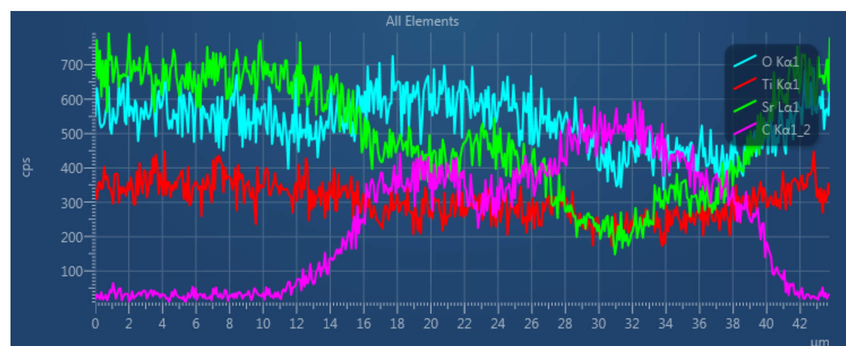

(b)

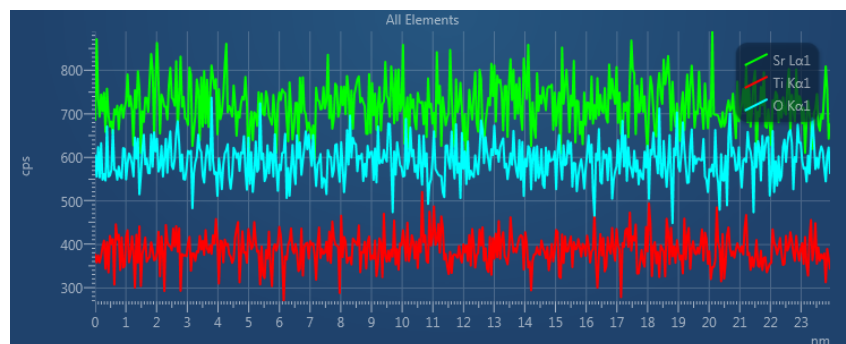

(c)

Figure 5.24: EDS line scans over TiO_2 thin films deposited by PLD on an untreated (a), new (b) and old (c) substrate. CPS varies greatly between the figures, and should not be used as a reference between the different figures, as these values were obtained by optimizing parameters for each sample individually. (b) was obtained from a line scan over a particle at the thin film surface.

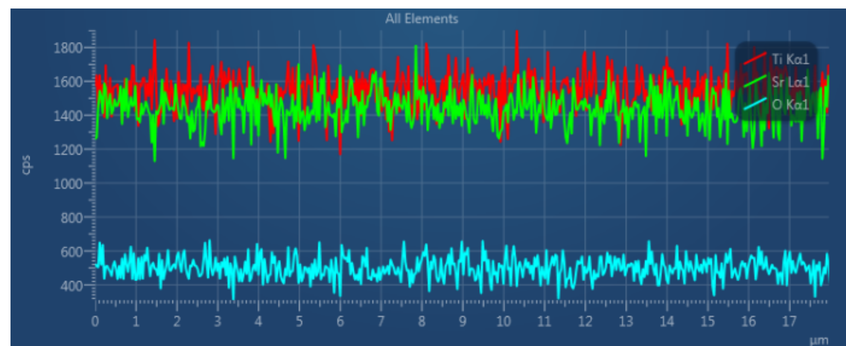

(a)

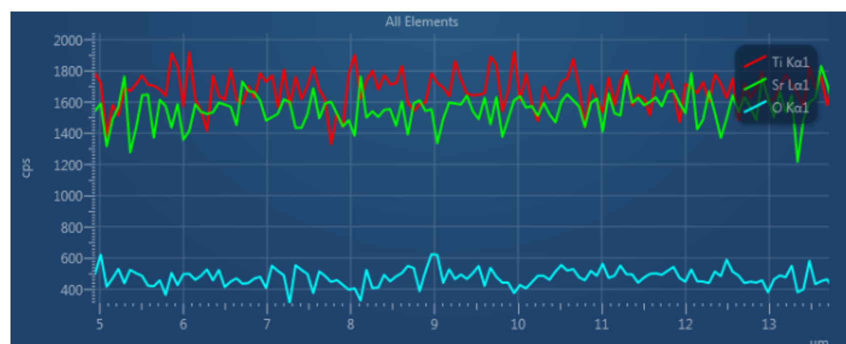

(b)

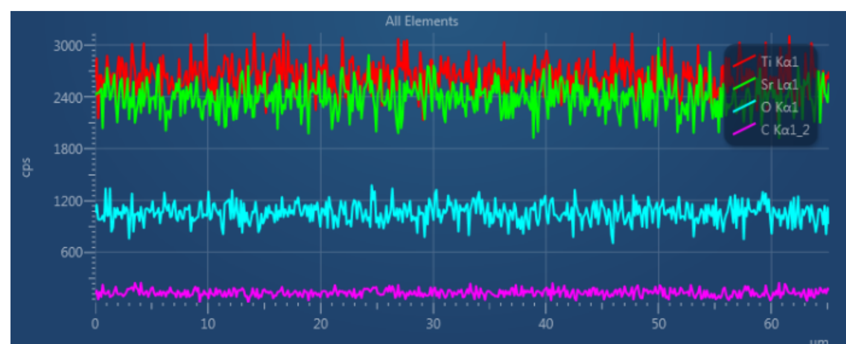

(c)

Figure 5.25: EDS line scans over TiO_2 thin films deposited by EBPVD on an untreated (a), new (b) and old (c) substrate. CPS varies greatly between the figures, and should not be used as a reference between the different figures, as these values were obtained by optimizing parameters for each sample individually.

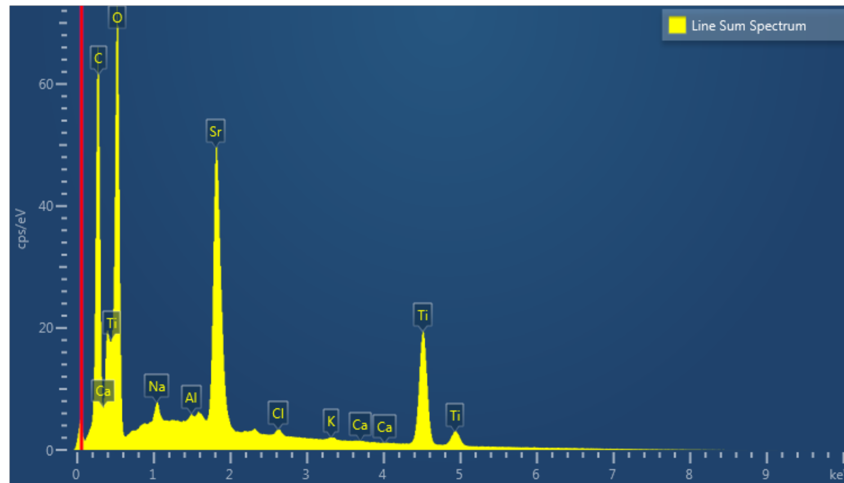

(a)

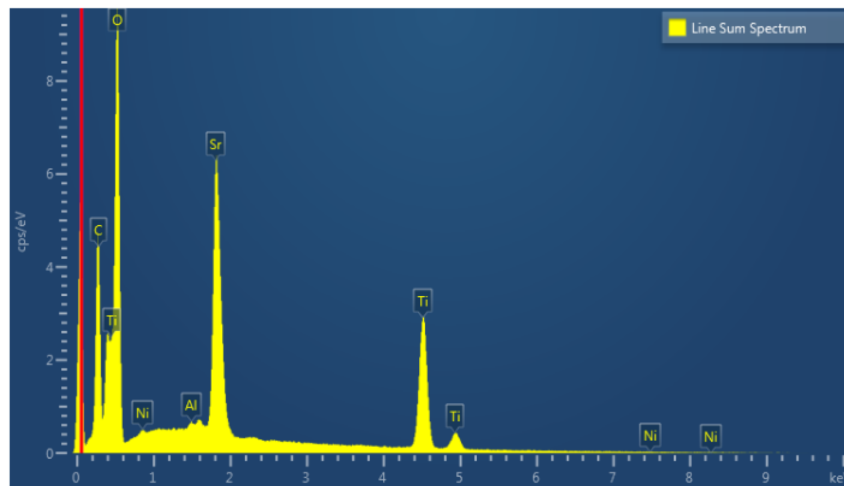

(b)

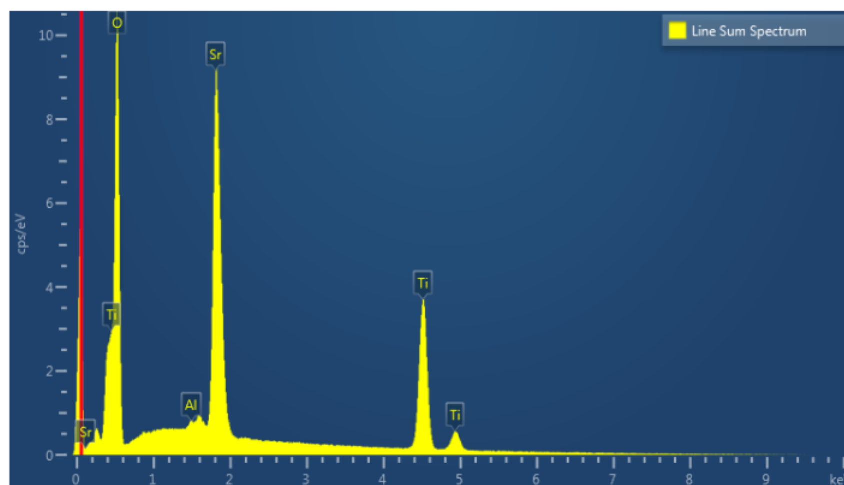

(c)

Figure 5.26: EDS line scans over TiO_2 thin films deposited by PLD on an untreated substrate (a), a new substrate (b) and an old substrate (c). CPS varies greatly between the figures, and should not be used as a reference between the different figures, as these values were obtained by optimizing parameters for each sample individually.

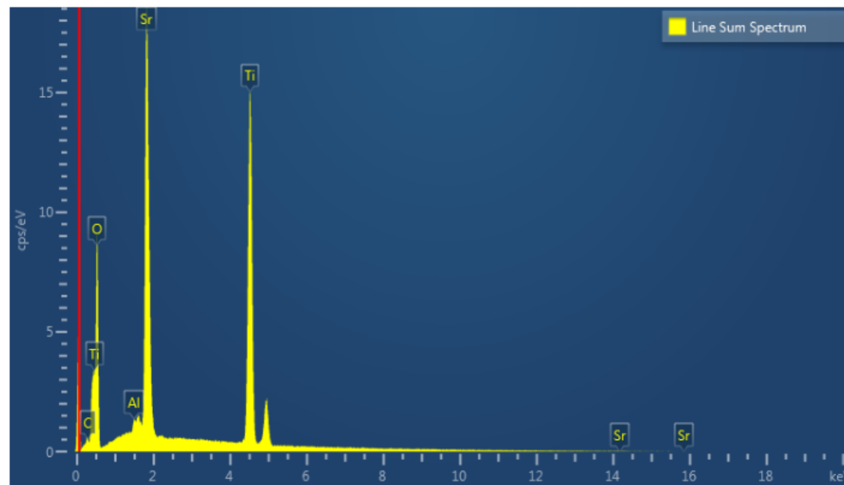

(a)

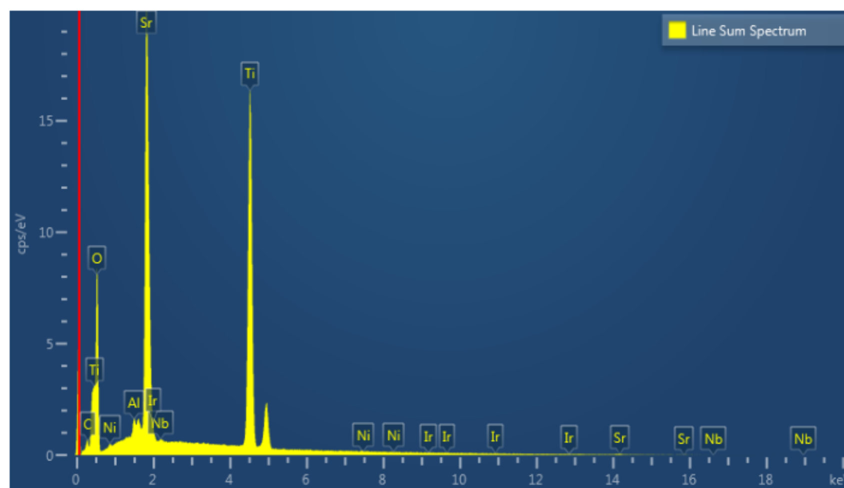

(b)

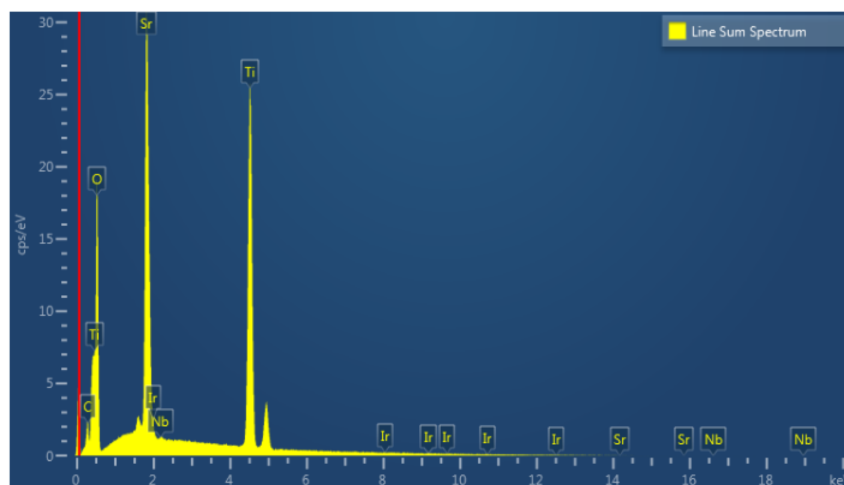

(c)

Figure 5.27: EDS line scans over TiO_2 thin films deposited by EBPVD on an untreated substrate (a), a new substrate (b) and an old substrate (c). CPS varies greatly between the figures, and should not be used as a reference between the different figures, as these values were obtained by optimizing parameters for each sample individually.

Chapter 6

Discussion

6.1 Substrate Surface Studies

6.1.1 Roughness and Inclination

The STO substrates purchased from the MTI Corporation are so called EPI-ready, meaning that they are ready for deposition of epitaxial thin films. However, looking at figure 5.1a, it is apparent that the surface is not flat at all, and would be unsuited for deposition. A substrate that had been kept in air for six weeks (see figure 5.1c) did not show the same structures as seen in figure 5.1a. This may indicate that the structures were some sort of external contamination. One possibility is that the contamination was caused by perturbation of strontium, as mentioned as a possibility by [14]. The surrounding area of the white specks in figure 5.1a appear as quite flat, and it may be this flat area that is imaged in figure 5.1c. Here, the surface appears very flat, but there are some indications of weird looking vertical structures in to upper right corner. Looking at the 2 μm^2 image on the six weeks old substrate (figure 5.1d), however, shows sign of steps, similar to the substrates described by [14]. The layers are not as uniform as the ones achieved using the preparation method of [14], which may lower the quality of a deposited thin film, meaning that preparation methods should be applied before deposition [12].

The acetone and isopropanol (AIP) method resulted in what looked like an almost destroyed substrate (see figure 5.2). Edges were not well-defined, and there were what appeared to be contaminations of some sort scattered across the surface, and it is safe to assume that these substrates would be unfit for deposition of thin films.

The weak waterleached substrate was not very well organized, but showed signs of step bunching, as seen in figure 5.3. This is in contrast with the findings of [14], who had well-defined planes after waterleaching just one time, and AFM imaging should have been performed at different locations on the substrate to make sure that the produced image was not an anomaly. Also, Connell et. al. mentions that some substrates may have step bunching, without any further explanation. It could then have proved useful to try the weak waterleaching method on a different substrate, to check if the step bunching was due to intrinsic

substrate properties, and not the preparation method used. The slope angle of the weak waterleached substrate, measured to 0°, might be a result of the levelling processes performed on the image, but the software might also not have a fine enough setting for calculating the actual slope. Assuming that the substrate indeed did have a slope, and by setting the lowest point on the substrate to 0 nm and the highest to 1.2 nm, it would be reasonable to expect a potential slope of $4.88 \cdot 10^{-5}$°, meaning that an approximate 0° seems quite reasonable.

Estimation of a potential slope can also be done by counting the number of planes, multiplying with the lattice constant and assuming that there is a slope going from the lowest to the highest point on the surface. This method, is however not recommended, as the atomic layers might consist of both TiO_2 and SrO planes, making for half integer steps. If we assume that the imaged layers in figure 5.3 are TiO_2 layers, this method will give us the approximate same value for the angle as before, when counting three planes, considering that $a = 3.905$Å. This information also leaves us with the impression that the substrate was TiO_2 terminated (integer step height), but the assumptions made are not to be trusted, and the software should always be used to estimate an inclination. Both the Gwyddion measurements, and the calculations are, however, very small, and close to 0, meaning that the substrate, most likely, could be considered as atomically flat.

The waterleach procedure was chosen for further studies, because the image in figure 5.4a was much closer to the results from [14] and because of a comparison with the weak waterleached, the AIP and untreated substrates. The waterleached substrates had well-defined edges and planes, and should be better suited for deposition of thin films than the other substrates. However, they were not as well-defined and uniform as the planes on the STO substrates used by [42].

As time went by, the roughness of the waterleached substrates appeared to increase, as seen in table 5.2, but the measurement of the six weeks old substrate was lower than the measurement of the three weeks old substrate, and the roughness of the new substrate was higher than that of the one week old. Remember now, that these substrates were not the same substrate as the one that was studied after one, two and three weeks, meaning that the results for zero and six weeks is not necessarily comparable to the one, two and three weeks old. The only observed tendency is that the roughness of the single substrate that was studied over time had an increase in surface roughness. The roughness increases by 40 % from one to two weeks, and another 36 % from two to three weeks, making for a total roughness increase of approximately 91 %. This might influence the properties of a deposited thin film, according to [12], and so, thin films deposited on these different roughness substrates should be characterized for the properties one wants to be able to reproduce. If the resulting thin films appear different, this might have been due to the increase in the roughness, indicating that the time between the substrate preparation and film deposition need to be reduced. The manufacturer, MTI, claimed that the STO substrates should have a roughness of less than 5 Å [43], meaning that all our substrates, including the untreated ones, were well within the given range.

In conclusion, the weak waterleached and waterleached substrates showed signs of well-defined planes and plane edges, whereas the substrates treated with acetone and isopropanol seemingly had a much less organized structure. Plane edges were not well-defined, almost smudged, but the roughness did not, however exceed that of a waterleached substrates three weeks after the treatment. Even though roughness parameters may vary to some degree with area at which measurements is taken and the number of data points used when imaging with the AFM, the fact that the roughness's are of the same order, indicates that the acetone and isopropanol treatment reduced surface roughness quite well, even though not quite as well as waterleaching. The substrate roughness seems to be quite dependent on the individual substrates.

The height of the steps in the images was calculated from the AFM measurements straight after the first waterleaching procedure. The value of (3.5±0.1) Å was less than expected. STO crystals have a lattice vector of 3.905 Å [9], most likely meaning that we had some issues with our measurements. A possible explanation is that the "Level data by fitting a plane through three points"-function in Gwyddion, was used to the best of it's capabilities. If there was noise in the image, a point through which the plane was fitted, may have been placed in such a way that it affected the entirety of the plane height. Another possibility is that the substrate was not crystalline at all, which could have been checked using XRD, but this seems less probable, seeing as there were well-defined planes. Other line scans, like the one in figure 5.5c also showed planes of lesser height, approximately (2.2±0.4) Å. This is approximately half of the lattice vector, and indicates that the layers seen in the AFM images are not necessarily the wanted TiO_2 layers, but alternating layers of SrO and TiO_2, meaning that the substrates were not completely TiO_2 terminated after all. Further water treatments may have helped in removing the remaining SrO layers, as described by [14].

The inclination of the substrate surface should be close to zero, according to the manufacturer of our substrates. This, however, was not the case for all the substrates. Some had a slope angle of up to 0.2°, meaning that the substrates had the same inclination to that of traditional mis-cut substrates, sold by companies such as the MTI corporation. The apparent inclination may also have been the result of our image processing.

The flat and well-defined planes were to be expected, from [14]. However, [14] experienced diffusion of strontium oxide to the surface one day after the second annealing, which again was removed when treating the substrate with DI water. Our substrates were waterleached straight after being cooled after the 2nd anneal, which may have stopped strontium oxide from diffusing.

6.1.2 Surface Composition

Our hopes for the XPS measurements on the waterleached substrates was that the new substrate would have a much lower presence of strontium oxide than the untreated one, indicating that the preparation had removed the strontium oxide layers from the substrate surface, making the substrate TiO_2 terminated. If there was less strontium on the new than the old

substrate, it would indicate that strontium might have diffused through the substrate as time went by (as described by [14]), but if the old substrate showed no presence of strontium, or at least the same amount as the newly treated substrate, it would indicate that the substrate was stable in regard to surface composition, and possibly in turn, termination, for at least six weeks. If there was a lot of strontium registered on the new substrate, this could indicate that the preparation possibly being inefficient, but seeing as XPS measures for up to 10 nm into a sample, we would expect strontium to be present, however, less than on the untreated substrate.

Although the survey scans proved quite similar, with the same spectrum materials appearing, as expected, the detailed scans showed more interesting features. In the scan over strontium, there was a clear presence of both strontium and strontium titanate at all three substrates, but the CPS was approximately 16 % higher for both the strontium and the strontium titanate peaks at the untreated substrate, indicated a higher presence of these materials at the surface, which indicates that the preparation method has had some effect.

The maximal peak of the oxygen spectrum on the untreated substrate (see figure 5.12b), located at 529.4 eV can correspond to both TiO_2 and STO, while the lower peaks (new and old substrates) matched well with TiO_2. Upon further inspection, it is possible to see a shift of approximately 0.1 eV between the peak of the untreated substrate, and the other two peaks, with the untreated substrate having the lowest binding energy. This can indicate that the untreated substrate peak being STO, while the two other peaks are more likely to be TiO_2, meaning that the treated substrates were of a higher TiO_2 termination, most likely caused by our preparation method. Then again, both possibilities are within the uncertainty of the measurements. Also, notice that the highest CPS on the lower peak (left shoulder in figure 5.12a) was made for the newly treated substrate, making for a better TiO_2 termination. The old substrate had the lowest CPS on this peak out of all the substrates, indicating that this substrate might not be as well suited for deposition of TiO_2 as the newly treated one.

The third scan, over the titanium peaks (figure 5.12c), showed the presence of two individual TiO_2 peaks. On this scan, however, the highest CPS was found in the untreated substrate, with a CPS approximately 5 % higher than that of the newly treated substrate, which in turn was approximately 1 % higher than the old one. In either case, all the substrates showed the presence if TiO_2 species at the surface, indicating that all the substrates were, to some degree, TiO_2 terminated. It was, however, not expected that the untreated substrate would have the highest amount of TiO_2.

All in all, the untreated substrates had higher reading at all the maximum peaks. The only peak where the untreated was not the strongest, was in the TiO_2 left shoulder peak on the oxygen scan.

6.1.3 Bulk and Surface Composition

Not surprisingly, energy dispersive X-ray spectroscopy (EDS), which penetrates deeper than XPS into samples, showed a large presence of both strontium, titanium and oxygen in all the

substrates. The amount of each material in each substrate seems to be quite equal when comparing the line scans in figure 5.14. According to basic chemistry, there should be three atoms of oxygen for every strontium and titanium atom ($SrTiO_3$), but the line scans indicates that oxygen is the less common element. This is most likely due to the fact that oxygen is a considerably lighter material than the two others. Strontium, being the heaviest material of the three, scatters a considerably larger amount of electrons, meaning that CPS for strontium will register as much higher than titanium and oxygen.

The sodium registered at all the substrates (see figure 5.13) is most probably caused by some form of contamination, either from the atmosphere or in one of the instruments. The carbon on the untreated substrate was, most likely, adventitious.

6.1.4 Improvements

The substrates may have been even flatter if we had heat annealed them for a longer time, and possibly letting them cool down at an even slower rate, by slowly reducing the heat in the oven. This might have reduced the speed of the recombination of the surface atoms, giving them more time to settle in positions making for a flatter surface [44]. Strontium oxide layers may have been removed to a larger degree if the substrates had been subject to the ultrasonic DI water bath for a longer period of time as suggested by [14]. XPS could have been performed on the same substrate over a period of a few weeks to check whether strontium would diffuse to the surface from lower layers in the substrate or not.

6.2 Thin Films

6.2.1 Thickness and Deposition Rate

The profilometer measurements were for the most part decent, except for the measurement of the old substrate. Several attempts were made at optimizing the scanning, but to no avail. Table 5.3 shows the thin film thicknesses and corresponding deposition rates. The new substrate demonstrates an approximate deposition rate quite similar to the deposition rate on the silicon substrate. The new substrate demonstrates a deposition rate 16.4 % higher than the untreated substrate. This might point towards the waterleaching preparation having a positive effect on the deposition rate, most likely due to a higher degree of TiO_2 termination, but it may as well have been caused by intrinsic differences in the substrates. Compared to previous experiments with our PLD instrument, the deposition rate was much lower [38], however these earlier experiments were made using a much higher fluence, and by holding the substrate in the centre of the plume during the entire deposition. We might have increased our deposition rate by increasing the fluence. Rotating the substrate holder slower would not have helped, as the substrates would have spent just as much time in every position either way.

6.2.2 Surface Composition

Three TiO_2 thin films were characterized by X-ray photoelectron microscopy. One deposited by PLD on a newly treated STO substrate, one by PLD on a silicon substrate and one by EBPVD on a newly treated STO substrate. The adventitious carbon peaks were located and all the data was moved by individual values to fit the adventitious carbon binding energy value of 284.8 eV.

From the spectra in figure 5.16 it is clear to see that variations in surface composition varies more as a function of the deposition technique than on the different substrates. There is, seemingly, one exception: In figure 5.16c we can clearly see silicon/silicon oxide peaks for thin films deposited by PLD on silicon and on the thin film deposited by EBPVD on the new STO substrate, whereas the TiO_2 thin film deposited by PLD on a new substrate show no sign of a peak. This effect was most likely caused by silicon contamination, as no similar features were found in my search in the literature. An optical microscope mounted in the XPS main chamber let us examine the STO substrate surface, and there were some particles, of unknown origin, located at the surface of the new substrate. The particles might have been silicon particles spread inside of the sample container, as the individual cells of the container were not completely isolated from the others.

The TiO_2 peaks resemble spectra other research teams have seen, such as [45] and [46]. The first of these had TiO_2 peaks at similar binding energies, but much more intense measurements, perhaps caused by a higher quality film, giving better response. The peaks were so intense that parts of them overlapped, whereas our peaks appear as separated. [46] ran XPS scans on a Cr-N codoped anatase TiO_2 PLD deposited thin film, but obtained similar results as our own, with two well defined and separated peaks.

The peaks of the PLD deposited thin films are shifted by a small amount from the maximum of the peak of the EBPVD deposited thin film (see figure5.16a and 5.16b). The shift is, however so small that the database values at these energies corresponded to the same materials.

6.2.3 Crystallinity

While all the PLD deposited films on STO substrates had the best crystalline match with rutile TiO_2, the PLD thin film rutile matching was quite bad, in the region of 44 % to 57 %. The thin film deposited on the silicon matched best with monoclinic Ti_3O_5 with a match of 59 %. This points towards the PLD thin films not being crystalline, as expected from previous work on room temperature PLD deposited TiO_2 thin films [47]. The amount of noise in the measurements could have been reduced by optimizing the scan parameters further, by finding the angles at which the thin films responded the best, and scanning slowly across these. The smoothing of the signal was done after the elemental matching in the software to create an easier to view tendency for the reader, however, the signal stayed quite rugged even after a smoothing factor of 3 had been applied.

The TiO_2 thin films deposited by electron-beam physical vapour deposition (EBPVD) on untreated and newly treated TiO_2 had matching with monoclinic TiO_2 in the range from 91 % to 97 %, whereas the thin film on the old substrate had its best match with monoclinic Ti_3O_5, with a matching of 67 %.

6.2.4 Surface Imaging and Bulk and Surface Composition

Energy dispersive X-ray spectroscopy was performed on all the thin films (see figure 5.23–5.27). As expected, the electrons penetrated not only the thin films, but also the substrate, which is why all line scans show the presence of strontium, except for the thin film deposited on silicon, which showed a large amount of silicon.

The thin film deposition by PLD on the untreated, new and old substrates all share the same characteristics: Oxygen and strontium is elements with the highest registered count, while titanium is a bit lower. In contrast to this, the EBPVD deposited thin films have more titanium and strontium than oxygen. As all these six films were deposited on STO, which is where the strontium was located, we can look away from the strontium in the graphs to get a better understanding of the thin film composition. Now it becomes clear that in the PLD on STO depositions, there is a much higher presence of oxygen than titanium, as oxygen has the highest CPS, but also the lowest response, while the EBPVD deposited thin films have a much lower presence of oxygen, with titanium being registered as the more abundant element, quite similarly to the substrates before the deposition.

Seeing as the profilometer measurements of the PLD thin film deposited on the new substrate gave an approximate thickness of 128 nm and that this thickness was enough to affect the EDS scan of the PLD deposited thin films in such an obvious manner, the EBPVD depositions might be very thin. Another possibility is that the oxygen atmosphere in the PLD main chamber made for films with a much higher degree of oxygen in them. An explanation of this might be that the oxygen in the PLD functions as a background gas, and is quite calm in the chamber, whereas the introduction of oxygen in the EBPVD main chamber happens through a tube quite near the substrate holder, not giving the oxygen atoms time to bond with the deposited thin film.

The PLD deposited thin films appeared, for the most part, as flat in the SEM images, in contrast with [47] who had larger particles of TiO_2 scattered across the substrate surface, when depositing TiO_2 at both room temperature and 500 °C. A TiO_2 particle, similar to the ones found by [47], was found at the TiO_2 thin film deposited on the silicon substrate.

Figure 5.21 shows how a particle of carbon registered in the EDS analysis. As seen in figure 5.21b the carbon covers an area similar to the area of the particle seen in figure 5.21a. The scan indicates that there is a presence of strontium and titanium beneath the particle, meaning that the particle was lying on top of the substrate. In figure 5.21d we can see that there are not only the expected strontium, titanium, oxygen and carbon peaks, but also calcium, sodium, aluminium, chlorine and potassium. The only elements appearing in figure 5.21c, however, is titanium, strontium, oxygen, carbon and sodium, probably due to a very

low CPS in the other elements. The appearance of these elements is most likely caused by some form of contamination, though we do not quite know what.

A challenge with the EBPVD deposition was that the deposition rate varied a great deal throughout experiment, most likely due to the fact that the electron beam burned evaporated a lot of the TiO_2 target, and that the target temperature varied as the electron beam moved through it.

Chapter 7

Conclusion

Strontium titanate substrates have been prepared using three different methods, where a method called waterleaching, consisting of heat annealing and ultrasonic DI water bathing of substrates performed two times, proved to be the best of the three alternatives. The surface of the substrate was found to have an increased TiO_2 termination after the waterleaching procedure by XPS characterization, but AFM imaging proved that the surface was not entirely TiO_2 terminated, as layers of strontium oxide rested between some of the TiO_2 layers. The roughness of the substrates appeared to increase as time went by, but the increase was not very large, in the pm-range, changes that should not affect the thin films in any dramatic way.

Thins films were deposited on untreated, newly treated and several weeks old STO substrates by PLD and EBPVD. A thin film of TiO_2 was also deposited on a silicon substrate. Profilometer measurements on the PLD deposited thin films gave ground to calculation of deposition rates on the substrates, and the tendency was that waterleached STO substrates had a higher deposition rate than an untreated substrate. The thin film deposited on the silicon substrate had a thickness similar to that of the thin film on the newly treated STO substrate, indicating that the deposition rate was not necessarily dependent on the substrate material. EDS showed that the PLD thin films deposited on STO substrates appeared to have a much higher content of oxygen than the thin films deposited by EBPVD. The PLD deposition on the silicon substrate showed that a particle of titanium was present at the surface of the deposited thin film.

SEM images of both the substrate and thin films showed relatively uniform surfaces, with small particles located at seemingly random positions on the sample surfaces. For the most part we found carbon particles, which might have been caused by some form of contamination from either instruments or other laboratory equipment, but we also found TiO_2 particles at the surface of the TiO_2 thin film deposited on a silicon substrate.

All in all, the waterleaching proved to improve the TiO_2 termination of STO substrates, but we did not reach complete TiO_2 termination. As expected, thin films deposited at room temperature by both PLD and EBPVD exhibit a low degree of crystallinity. PLD deposition proved to create thin films with a much higher oxygen content than EBPVD deposition.

Chapter 8

Suggestions for Future Work

It would be interesting to deposit a TiO_2 thin film on a 2.5 inch STO wafer to get a feel of the deposition rate as a function of the distance from the centre of the plume. This would have had to be done while holding the substrate still, and would be of great help in future PLD deposition experiments, as it would make it easier to calculate an estimated thin film thickness before a deposition.

In regard to substrate preparation, the ultrasonic DI water bath should be performed for a longer time, up to several minutes, to check if this affects the STO surface termination further than what was the case for the time intervals we have used. Substrates should also be prepared by HF etching, to check if such a preparation method has an advantage over the waterleaching. Characterization of these substrates should at the very least be performed using AFM. If possible, it would also be interesting to perform XPS time studies of the substrates. Models could be developed for the decay of the STO substrate surfaces and be compared, to find out if the preparation method affects the time the substrate surface remains stable or if this is an intrinsic property of the material. If a model could be developed, it could also help in estimating the lifetime of a substrate surface which would be of great use in the future.

Spectroscopic ellipsometry can be performed on both the substrates and potential thin films, both to estimate film thickness and to make calculations of the surface roughness. It may also be used to measure other quantities, such as reflective index if needed.

Bibliography

[1] A. E. Brand, S. M. Chekardovskiy, and K. A. Akulov. The Analysis of the Development Dynamics and Structural Balance of Solar Energy in the World. *IOP Conference Series: Earth and Environmental Science*, 50(1):012034, 2017.

[2] Gavin Conibeer. Third-generation photovoltaics. *Materials Today*, 10(11):42 – 50, 2007.

[3] E. Antolín, A. Martí, and A. Luque. 1.29 - intermediate band solar cells. In Ali Sayigh, editor, *Comprehensive Renewable Energy*, pages 619 – 639. Elsevier, Oxford, 2012.

[4] Antonio Luque and Antonio Martí. Increasing the efficiency of ideal solar cells by photon induced transitions at intermediate levels. *Physical Review Letters*, 78(26):5014, 1997.

[5] Fara, Laurentiu, Yamaguchi, and Masafumi. *Advanced Solar Cell Materials, Technology, Modeling and Simulation.* IGI Global, 2013.

[6] Anouar Hajjaji, Mosbah Amlouk, Mounir Gaidi, Brahim Bessais, and My Ali El Khakani. *Chromium Doped TiO_2 Sputtered Thin Films: Synthesis, Physical Investigations and Applications.* Springer, 2014.

[7] Fengcheng Wu, Haiping Lan, Zhenyu Zhang, and Ping Cui. Quantum efficiency of intermediate-band solar cells based on non-compensated np codoped TiO_2. *The Journal of chemical physics*, 137(10):104702, 2012.

[8] Charles Kittel. *Introduction to Solid State Physics.* Wiley, 8 edition, 2005.

[9] John W. Anthony, Richard A. Bideaux, Kenneth W. Bladh, and Monte C. Nichols. *Handbook of Mineralogy: Halides, Hydroxides, Oxides.* Mineral Data Pub, 1997.

[10] Ole Gobel. *The growth of patterned ceramic thin films from polymer precursor solutions.* PhD thesis, University of Groningen, 2004.

[11] C. Raisch, T. Chasse, C. Langheinrich, and A. Chasse. Preparation and investigation of the A-site and B-site terminated $SrTiO_3$(100) surface: A combined experimental and theoretical x-ray photoelectron diffraction study. *Journal of Applied Physics*, 112(7):073505, 2012.

[12] S. F. Cui, Z. H. Mai, H. Zhou, C. G. Cui, D. Y. Dai, C. Y. Wang, L. S. Wu, S. F. Zhang, Y. Z. Zhang, Y. Y. Zhao, L. Li, B. C. Yang, and X. P. Wang. Study of the correlations between the critical current density and the structures of $YBa_2Cu_3O_{7-\delta}$ thin films. *Superconductor Science and Technology*, 4(7):279, 1991.

[13] Gertjan Koster, Guus Rijnders, Dave H.A. Blank, and Horst Rogalla. Surface morphology determined by (001) single-crystal $SrTiO_3$ termination. *Physica C: Superconductivity*, 339(4):215 – 230, 2000.

[14] J. G. Connell, B. J. Isaac, G. B. Ekanayake, D. R. Strachan, and S. S. A. Seo. Preparation of atomically flat $SrTiO_3$ surfaces using a deionized-water leaching and thermal annealing procedure. *Applied Physics Letters*, 101(25):251607, 2012.

[15] Qidu Jiang and Jörg Zegenhagen. $SrTiO_3$(001)-c(6 × 2): a long-range, atomically ordered surface stable in oxygen and ambient air. *Surface Science*, 367(2):L42 – L46, 1996.

[16] R. Takahashi, Y. Matsumoto, T. Ohsawa, M. Lippmaa, M. Kawasaki, and H. Koinuma. Growth dynamics of the epitaxial SrO film on $SrTiO_3$(001). *Journal of Crystal Growth*, 234(2):505 – 508, 2002.

[17] M. Kawasaki, A. Ohtomo, T. Arakane, K. Takahashi, M. Yoshimoto, and H. Koinuma. Atomic control of $SrTiO_3$ surface for perfect epitaxy of perovskite oxides. *Applied Surface Science*, 107:102 – 106, 1996. Proceedings of the Third International Symposium on Atomically Controlled Surfaces and Interfaces.

[18] T. Kubo and H. Nozoye. Surface structure of $SrTiO_3$(100). *Surface Science*, 542(3):177 – 191, 2003.

[19] Q.D. Jiang and J. Zegenhagen. $SrTiO_3$(001) surfaces and growth of ultra-thin $GdBa_2Cu_3O_{3-x}$ films studied by LEED/AES and UHV-STM. *Surface Science*, 338(1):L882 – L888, 1995.

[20] Hiroaki Nishikawa, Masaki Kanai, and Tomoji Kawai. Heteroepitaxy of perovskite-type oxides on oxygen-annealed $SrTiO_3$(100). Important factors for preparation of atomically flat oxide thin films. *Journal of Crystal Growth*, 179(3):467 – 476, 1997.

[21] Lifeng Liu, Huibin Lu, Yiyan Fei, Haizhong Guo, Wenfeng Xiang, and Zhenhao Chen. Formation of atomically smooth surfaces on $SrTiO_3$ substrates for epitaxial film growth. *Journal of Crystal Growth*, 253(1):374 – 377, 2003.

[22] P. Sohrabi, S. Daneshmandi, H. Salamati, and M. Ranjbar. Pulsed laser deposition of $La_{0.6}Ca_{0.4}Fe_{0.8}Ni_{0.2}O_{3-\delta}$ thin films on $SrTiO_3$: Preparation, characterization and electrical properties. *Thin Solid Films*, 571:180–186, 2014.

[23] Michio Naito and Hisashi Sato. Reflection high-energy electron diffraction study on the $SrTiO_3$ surface structure. *Physica C: Superconductivity*, 229(1):1 – 11, 1994.

[24] D. M. Mattox. *Handbook of Physical Vapor Deposition (PVD) Processing.*, volume 2nd ed. William Andrew, 2010.

[25] Douglas B. Chrisey and Graham K. Hubler. *Pulsed Laser Deposition of Thin Films.* Wiley, New York, 1994. A Wiley-Interscience publication.

[26] Greg Haugstad. *Atomic Force Microscopy.* Wiley, 2012.

[27] Bruker AFM Probes. SCANASYST-AIR. `http://www.brukerafmprobes.com/p-3726-scanasyst-air.aspx`. [Online; accessed 28-05-2017].

[28] Nicholas A. Geisse. AFM and combined optical techniques. *Materials Today*, 12(7–8):40 – 45, 2009.

[29] G. K. Bennig. Atomic force microscope and method for imaging surfaces with atomic resolution, February 9 1988. US Patent 4,724,318.

[30] C. Oliver Wells. *Scanning Electron Microscopy.* McGraw-Hill, New York, 1974.

[31] James Pawley and Heide Schatten. *Biological Low-Voltage Scanning Electron Microscopy.* Springer, New York, 2007. Retrieved from http://site.ebrary.com/lib/ntnu/detail.action?docID=10217696 on Dec. 5th, 2016.

[32] Paul van der Heide. *X-ray Photoelectron Spectroscopy.* Wiley, 2012.

[33] Gerd Binnig, Calvin F Quate, and Ch Gerber. Atomic force microscope. *Physical review letters*, 56(9):930, 1986.

[34] Kaimin Shih. *X-ray Diffraction : Structure, Principles, and Applications.* Nova Science Publishers, Inc, 2013.

[35] Bernard Borie. X-Ray Diffraction in Crystals, Imperfect Crystals, and Amorphous Bodies. *Journal of the American Chemical Society*, 87(1):140–141, 1965.

[36] Pulak Dutta. Grazing incidence X-ray diffraction. *Curr. Sci*, 2000:1478–1483, 2000.

[37] Kurt J. Lesker Company. Frequently Asked Questions. `http://www.lesker.com/newweb/faqs/question.cfm?id=152`. [Online; accessed 24-06-2017].

[38] E. Hannaaas. *Initial studies of ablation of TiO_2 and deposition of TiO_2 and CrN.* Project work, NTNU, Trondheim, Norway, 2016.

[39] Gwyddion. Gwyddion. `http://gwyddion.net/`. [Online; accessed 19-02-2017].

[40] NorFab. SEM APREO. `http://ntnu.norfab.no/WebForms/Equipment/EquipmentView.aspx?toolId=96`. [Online; accessed 24-06-2017].

[41] NIST. X-ray Photoelectron Spectroscopy Database, Version 4.1 (National Institute of Standards and Technology, Gaithersburg, 2012. http://srdata.nist.gov/xps/, 2012. [Online; accessed 24-06-2017].

[42] Alessio Giampietri, Giovanni Drera, Igor Píš, Elena Magnano, and Luigi Sangaletti. Tracking the amorphous to epitaxial transition in RF-sputtered cubic BFO-STO heterojunctions by means of X-ray photoelectron diffraction. *Applied Physics Letters*, 109(13):132903, 2016.

[43] MTI Corporation. $SrTiO_3$ (100) 10x10x0.5 mm Epi polished wafer 2SP. http://www.mtixtl.com/STO-a-101005S2.aspx, 2017. [Online; accessed 01-07-2017].

[44] M. Kareev, S. Prosandeev, J. Liu, C. Gan, A. Kareev, J.W. Freeland, Min Xiao, and J. Chakhalian. Atomic control and characterization of surface defect states of TiO_2 terminated $SrTiO_3$ single crystals. *Applied Physics Letters*, 93(6):061909, 2008.

[45] G. Soto. AES, EELS and XPS characterization of Ti(C, N, O) films prepared by PLD using a Ti target in N_2, CH_4, O_2 and CO as reactive gases. *Applied Surface Science*, 233(1):115 – 122, 2004.

[46] Yang Wang, Zhengwang Cheng, Shijing Tan, Xiang Shao, Bing Wang, and J.G. Hou. Characterization of Cr–N codoped anatase TiO_2(001) thin films epitaxially grown on $SrTiO_3$(001) substrate. *Surface Science*, 616:93 – 99, 2013.

[47] Sin-iti Kitazawa, Yeongsoo Choi, and Shunya Yamamoto. In situ optical spectroscopy of PLD of nano-structured TiO_2. *Vacuum*, 74(3):637 – 642, 2004. Selected papers revised from the Proceedings of the Seventh International Symposium on Sputtering and Plasma Processes (ISSP 2003).

Appendix A

SEM Images of Surface Particles at TiO_2 Thin Films

Images of particles found on the surface of the EBPVD deposited TiO_2 thin films are shown in figure A.1 and A.2. The particles found on the PLD deposited TiO_2 thin films are shown in figure A.3. All imaging was done using secondary electrons in the FEI SEM APREO.

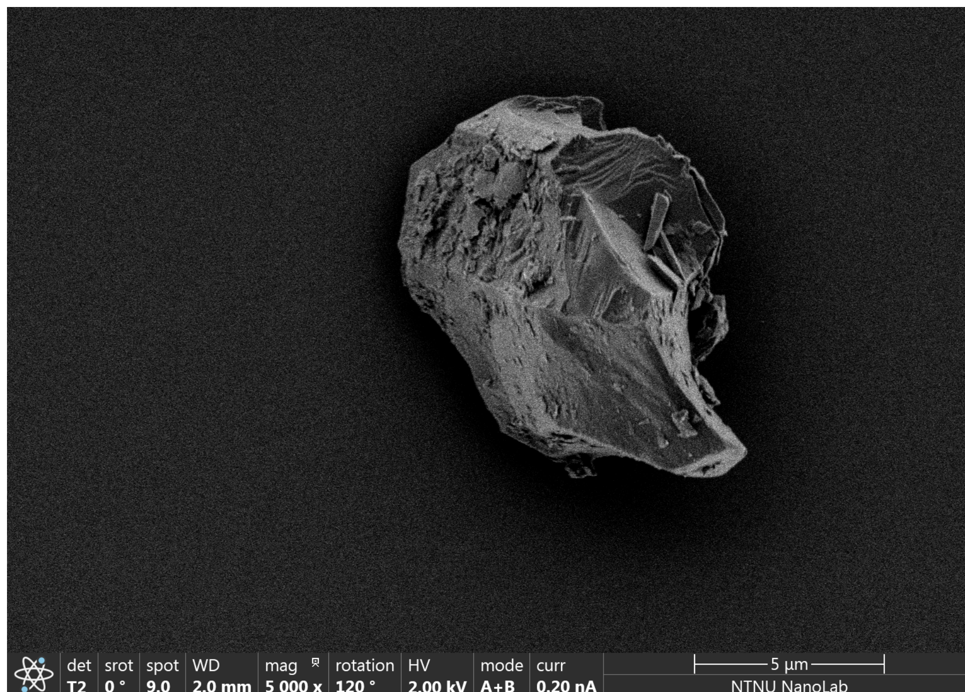

(a)

Figure A.1: SEM image of a particle at the surface of TiO_2 thin films deposited by EBPVD on an untreated substrate.

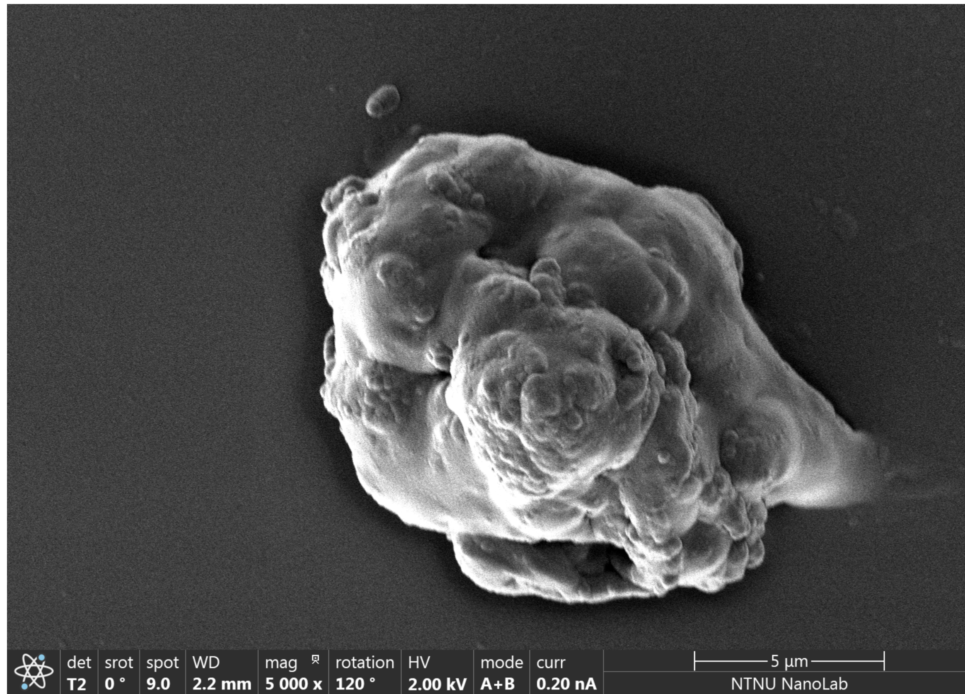

(a)

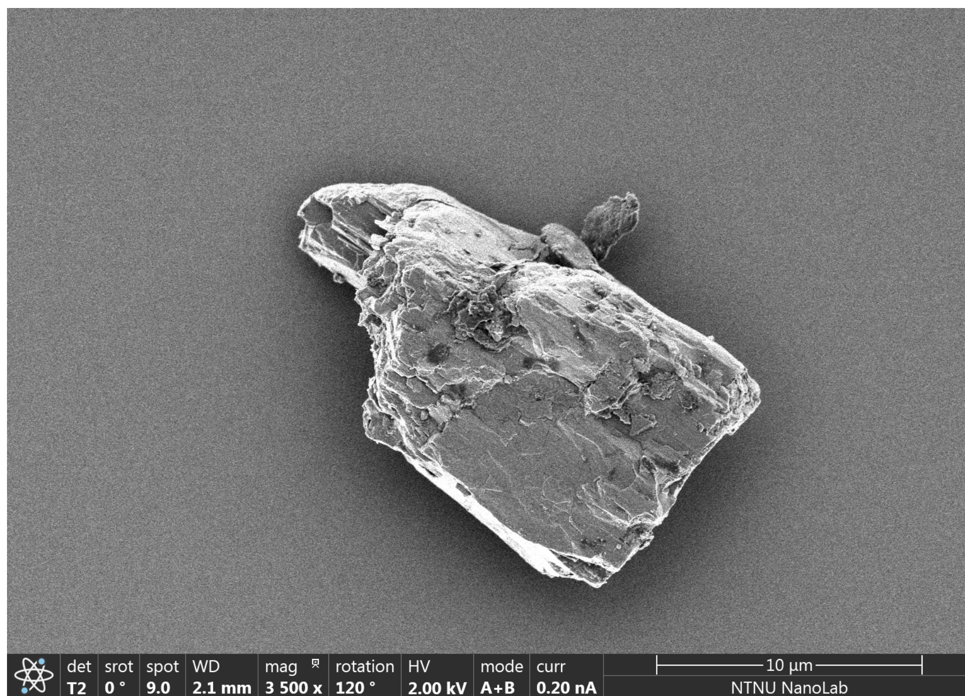

(b)

Figure A.2: SEM images of particles at surface of TiO_2 thin films deposited by EBPVD on newly treated (left) and old treated (right) substrates.

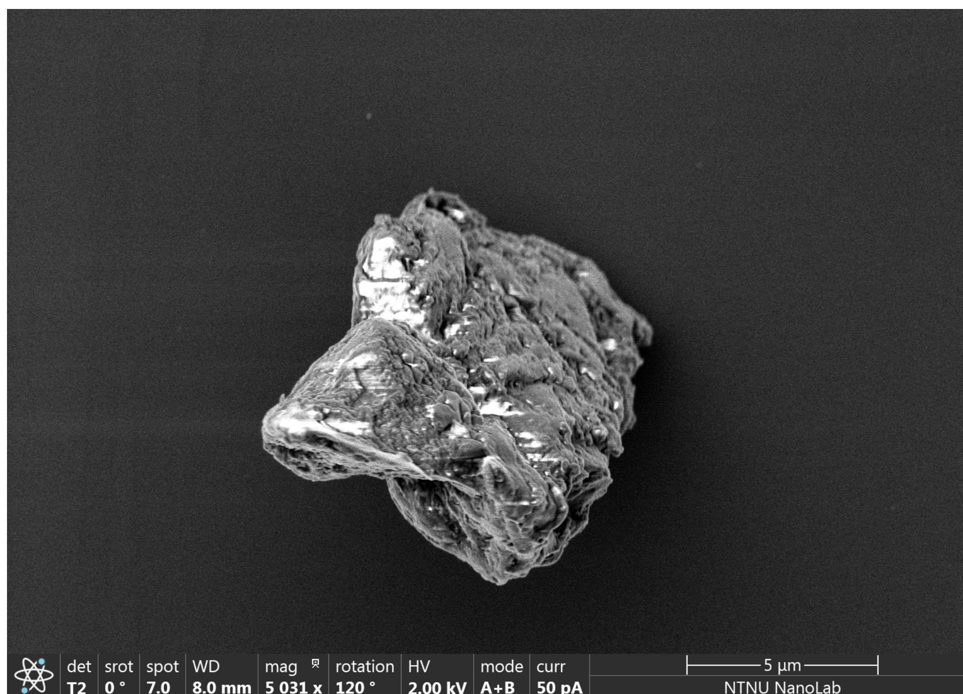

(a)

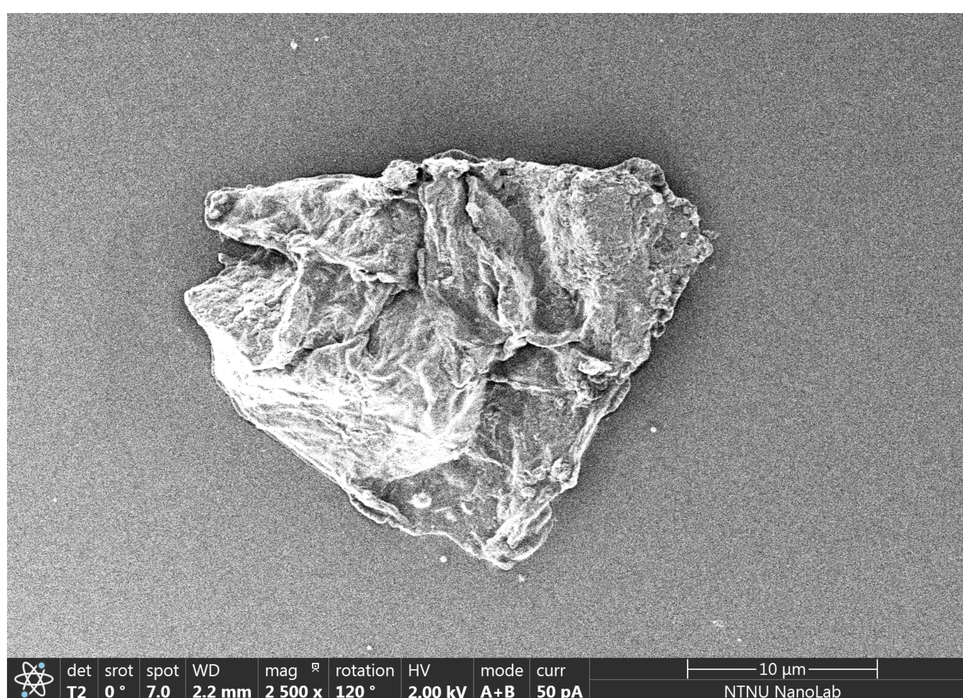

(b)

Figure A.3: SEM images of particles at surface of TiO_2 thin films deposited by PLD on untreated (a) and newly treated (b) STO substrates.

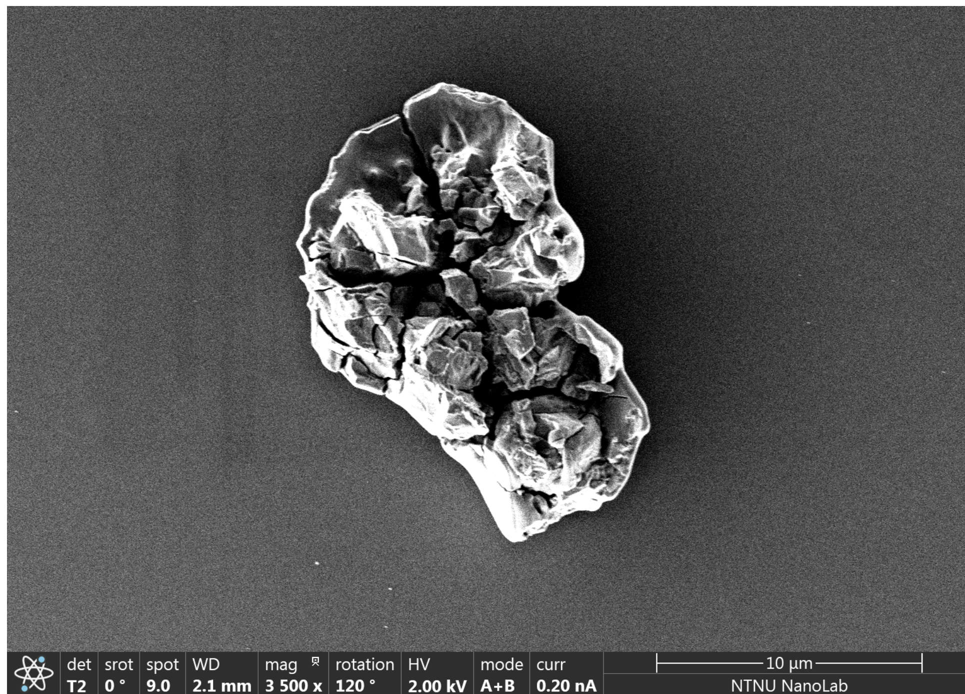

(a)

(b)

Figure A.4: SEM images of particles at surface of TiO_2 thin films deposited by PLD on old treated STO (a) and silicon (c) substrates.